Article

Current Biology

# Distinct Neural Circuits Control Rhythm Inhibition and Spitting by the Myogenic Pharynx of *C. elegans*

## Highlights

- Three neural circuits modulate and alter *C. elegans* pharyngeal pumping
- One intrinsic circuit inhibits pumping, whereas another promotes spitting
- A third circuit relays a signal from outside its organ, like the autonomic system
- Functional synapses can exist despite the absence of a synapse in the connectome

## Authors

Nikhil Bhatla, Rita Droste, Steven R. Sando, Anne Huang, H. Robert Horvitz

## Correspondence

horvitz@mit.edu

## In Brief

How do neural circuits modulate myogenic muscle organs that can beat on their own, such as the heart? Bhatla et al. describe how the function of a myogenic muscle organ of *C. elegans*, the pharynx, is inhibited by two neural circuits and dramatically altered by a third, which transforms swallowing into spitting.

Bhatla et al., 2015, Current Biology *25*, 2075–2089
August 17, 2015 
http://dx.doi.org/10.1016/j.cub.2015.06.052

CellPress

Current Biology
Article

# Distinct Neural Circuits Control Rhythm Inhibition and Spitting by the Myogenic Pharynx of *C. elegans*

Nikhil Bhatla,[1,2] Rita Droste,[1] Steven R. Sando,[1] Anne Huang,[1] and H. Robert Horvitz[1,*]
[1]Howard Hughes Medical Institute, Department of Biology, McGovern Institute for Brain Research
[2]Department of Brain and Cognitive Sciences
Massachusetts Institute of Technology, 77 Massachusetts Avenue, Cambridge, MA 02139, USA
*Correspondence: horvitz@mit.edu
http://dx.doi.org/10.1016/j.cub.2015.06.052

## SUMMARY

**Neural circuits have long been known to modulate myogenic muscles such as the heart, yet a mechanistic understanding at the cellular and molecular levels remains limited. We studied how light inhibits pumping of the *Caenorhabditis elegans* pharynx, a myogenic muscular pump for feeding, and found three neural circuits that alter pumping. First, light inhibits pumping via the I2 neuron monosynaptic circuit. Our electron microscopic reconstruction of the anterior pharynx revealed evidence for synapses from I2 onto muscle that were missing from the published connectome, and we show that these "missed synapses" are likely functional. Second, light inhibits pumping through the RIP-I1-MC neuron polysynaptic circuit, in which an inhibitory signal is likely transmitted from outside the pharynx into the pharynx in a manner analogous to how the mammalian autonomic nervous system controls the heart. Third, light causes a novel pharyngeal behavior, reversal of flow or "spitting," which is induced by the M1 neuron. These three neural circuits show that neurons can control a myogenic muscle organ not only by changing the contraction rate but also by altering the functional consequences of the contraction itself, transforming swallowing into spitting. Our observations also illustrate why connectome builders and users should be cognizant that functional synaptic connections might exist despite the absence of a declared synapse in the connectome.**

## INTRODUCTION

Animals rely on muscles for functions critical to their lives, from the execution of behavior to internal processes such as digestion and circulation. In general, animals have two kinds of muscles. The first requires neural activity to contract, such as skeletal muscle. The second, myogenic muscle, does not require neural activity to contract, and neural activity instead serves a modulatory role. Cardiac muscle, including cardiomyocytes, and some enteric muscles are myogenic [1, 2], and input from the autonomic nervous system plays a modulatory role, such as altering heart rate [3]. Understanding the logic of such modulatory neural circuits requires an understanding at the cellular level, which can be difficult to achieve in vertebrates.

We sought to investigate neural control of a myogenic muscle organ in an organism readily amenable to cellular and molecular analyses. Neural circuits in invertebrates can be understood in a "gap-free" manner, meaning that the function of each individual neuron that contributes to a larger neural circuit can be identified [4–6]. We selected the nematode *Caenorhabditis elegans* to study neural control of myogenic muscles because (1) its nervous system has only 302 neurons, (2) its connectome (the putatively complete set of all anatomical synapses among all neurons) has been described [7, 8] and is easily accessed [9], (3) neural circuits can be examined at the cellular level in vivo, and (4) neural circuits can be analyzed at the molecular level using genetic methods.

The *C. elegans* pharynx is a myogenic muscle group that functions as the worm's feeding organ, pumping bacteria into the intestine [10]. The pharyngeal nervous system consists of 20 neurons of 14 classes, and, as with the heart, neural innervation serves a modulatory rather than necessary role for pumping [11]. Physiological or behavioral functions have been described for nine neuron classes (MC, M2, M3, M4, I1, I2, I4, I5, and NSM) [11–17].

We previously reported that short wavelength light (violet and UV) interrupts the pumping rhythm of the pharynx and suggested that light generates hydrogen peroxide or another reactive oxygen species that is toxic to the worm [16]. In an effort to reduce exposure to the toxic effects of light, the worm inhibits feeding and avoids the light [18–20]. Here, we use the inhibition of *C. elegans* pumping in response to light as a tool to analyze how neurons control the worm's myogenic muscular pump, the pharynx. By studying this behavioral response using cellular and molecular methods, we identify three neural circuits that control this myogenic muscle organ.

## RESULTS

### The I2 Pharyngeal Neurons Can Function as Sensory Neurons

In the presence of food, the *C. elegans* pharynx pumps rapidly (4 to 5 Hz). Short-wavelength light (436 nm; 13 mW/mm$^2$) alters pumping in three distinct phases, as previously reported [16]. First, pumping rapidly stops in response to light (the "acute" response; 0–5 s after light onset). Second, pumping subsequently increases in the continued presence of light (the

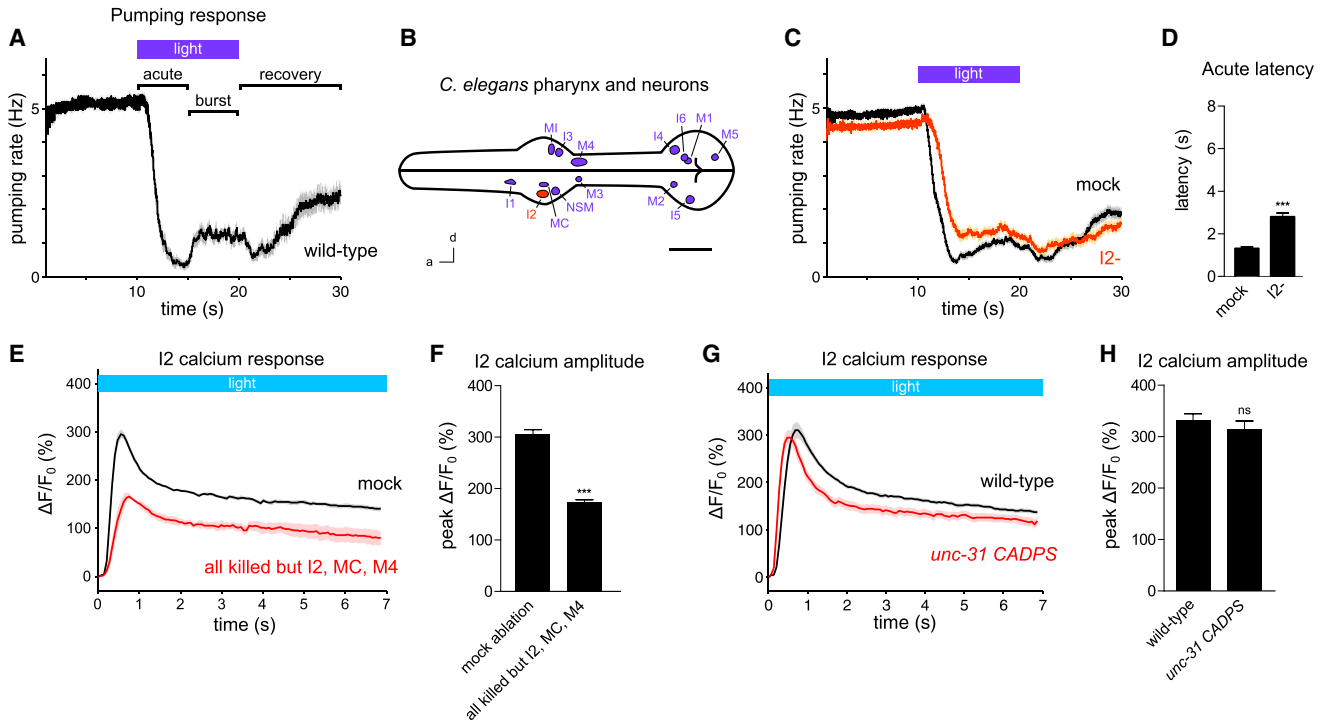


**Figure 1. The I2 Pharyngeal Neurons Can Function as Sensory Neurons**

(A) Pumping response to 436 nm (13 mW/mm$^2$) light, with the acute, burst, and recovery responses labeled. This result was previously described [16]. n = 20 worms. For all legends, if the number of trials is unspecified, each worm or cell was assayed once.

(B) Map of pharyngeal neuron nuclei; 14 of the 20 total neurons are shown, as neurons that are members of a pair are depicted as a single neuron. I2 is highlighted in red. a, anterior; d, dorsal. The scale bar represents 15 μm.

(C) I2 ablation caused a defect in the acute response to light. n = 72 trials, 32 worms. Reproduced from [16].

(D) Quantification of acute response latency. Reproduced from [16].

(E) I2 responds to light in worms in which all pharyngeal neurons except I2, MC, and M4 have been ablated with a laser. n = 3 neurons.

(F) Quantification of the peak calcium response in I2.

(G) *unc-31(u280) CADPS* mutants, which are defective in humoral signaling, exhibit an I2 calcium response similar to that of the wild-type. n = 22 neurons.

(H) Quantification of the peak calcium response in I2.

The calcium response was measured in the posterior neurite of I2. Error bars and shading around traces indicate SEM. ***$p < 0.001$; ns, not significant at $p < 0.05$; t test compared to mock-ablated control or wild-type.

See also Figure S1.

"burst" response; 5–10 s after light onset). Third, pumping slowly begins to recover after light is removed (the "recovery" response; 0–10 s after light removal; Figure 1A).

Previously, we showed that loss of the I2 pharyngeal neuron pair (Figure 1B) causes a partial defect in the acute response to light (Figures 1C and 1D) [16]. In addition, light causes an increase in I2 calcium [16]. We concluded that I2 executes part of the acute response to light.

The increase in I2 calcium caused by light could result either from I2's receiving a signal from another cell or from I2's directly sensing light without a cellular intermediary. If I2 receives a signal from another cell, that signal could be communicated either via a direct synapse or humorally. To identify candidate neurons that directly synapse onto I2, we examined the connectome of the pharynx [7]. The I1 neuron pair and the M1 neuron were reported to form gap junctions with or provide chemical synaptic input to I2. Our connectome analysis (see below) suggested that the original connectome might be missing functional synapses, so we used a laser to ablate all pharyngeal neurons that would not affect the worm's growth or health; specifically, the MC neuron pair, which promotes pumping, and the M4 neuron, which promotes peristalsis, were not killed [11, 12]. Altogether, 15 of 20 pharyngeal neurons were killed in each worm. Ablated worms exhibited an I2 response at 56% of the level of mock-ablated worms (Figures 1E and 1F). This result shows that I2 can respond to light in the absence of 11 of 13 pharyngeal neuron classes, although part of the I2 response depends on other pharyngeal neurons.

We next sought to determine whether the I2 response to light requires a humoral signal. Humoral signaling is partially mediated by dense-core vesicle release, which requires UNC-31, the worm ortholog of human CADPS/CAPS [21]. Putative null mutants of *unc-31(u280)* showed an I2 response similar to that of wild-type (Figures 1G and 1H), suggesting that I2 does not receive a dense-core vesicle-mediated signal to trigger its response to light. Because neither direct synaptic input nor dense-core vesicle input appears to be necessary for I2 to respond to light, I2 likely senses light without a neuronal intermediary.

A third reason to think that I2 functions as a cellular sensor for light is that it expresses a putative molecular sensor for a

light-generated molecule, hydrogen peroxide. The molecular receptor GUR-3 functions in I2 to detect hydrogen peroxide and increase calcium [16]. Taking these results together, we conclude that the I2s can function as sensory neurons, although the I2 response to light is also modulated by other pharyngeal neurons.

To identify regions of I2 that when exposed to light are sufficient to induce the cellular response, we restricted light to the anterior neurite, the soma, or the posterior neurite (Figure S1A). We found that illumination of the posterior neurite caused a large increase in fluorescence throughout I2, whereas anterior neurite or soma illumination caused little increase in fluorescence (Figures S1B–S1D). To determine which of the two neurites is necessary for the light-induced response, we cut the anterior or posterior neurite using a laser, killing the severed neurite, and then exposed the worm's head to light. We found that I2 responded in the absence of either the anterior or the posterior neurite, although the response in the anterior neurite after the posterior neurite was cut was significantly smaller than the response in the anterior neurite in the intact control (Figures S1E–S1H). Overall, these results suggest that, whereas the posterior neurite is the most light-sensitive compartment, the soma and anterior neurite are also light sensitive and can be sufficient to trigger an influx of calcium into I2.

## I2 Activation Depends in Part on the Voltage-Gated Calcium Channels UNC-2 and UNC-36

To determine the molecular source of the increase in I2 calcium in response to light, we tested mutants disrupted in calcium influx. Although most of these mutants had a normal I2 response (Figures S2A–S2G), we found that mutants carrying nonsense alleles of *unc-2*(*e55*) ($\alpha_1$ subunit; N/P/Q-type voltage-gated calcium channel [VGCC]) [22] or *unc-36*(*e251*) ($\alpha_2\delta$ subunit; VGCC) [23] exhibited a partial defect: the calcium response latency was approximately doubled and the peak amplitude of the response was approximately halved (Figures 2A, 2B, 2D, and 2E). The *unc-36*; *unc-2* mutant was no more defective in the I2 response than the *unc-2* mutant (Figures 2C–2E), suggesting that *unc-2* and *unc-36* function in the same pathway.

We next assayed the pumping response of calcium channel mutants to determine whether any mutant exhibited an acute response defect similar to I2-ablated animals. Whereas several mutants showed differences from wild-type in the burst and recovery responses (Figures 2F, 2G, and S2H–S2N), only *unc-36* mutants exhibited a small but statistically significant defect in the latency of the acute response to light (Figures 2G, 2I, and 2J). *unc-36*; *unc-2* double mutants had a latency defect similar to that of *unc-36* mutants (Figures 2H–2J). In addition, the remaining double mutants among *unc-36*, *unc-2*, *egl-19*, and *cca-1* were either wild-type or no more defective than *unc-36* or *unc-2* mutants in the I2 response (Figures S2O–S2S). Finally, the *unc-36*; *egl-19*; *cca-1* triple mutant was only modestly more defective than the *unc-36* single mutant in the I2 response (Figure S2T). We conclude that *unc-2* and *unc-36* are partially required for the I2 calcium response to light and likely function in the same pathway.

## The I2 Neurons Are Glutamatergic

To identify cells downstream of I2, we took a molecular approach and sought to determine the neurotransmitter(s) that I2 secretes, the receptor(s) functioning downstream, and the cells in which the receptor(s) functions. Whereas most neurotransmitter mutants showed a normal acute pumping response to light (Figures S3A–S3H), mutants defective in glutamate neurotransmission because of a deletion in *eat-4* (allele *ky5*), a vesicular glutamate transporter (*VGLUT*) [24], exhibited a severe defect in the latency and amplitude of the acute response (Figures 3A, 3E, and 3F). Multiple alleles of *eat-4* (*n2458*, *n2474*, *ad819*, *ad572*, and *ok2233*) exhibited a similar defect (data not shown), and a genomic *eat-4* transgene (*njEx378*) [25] fully rescued the defect of *eat-4*(*ky5*) mutants (Figures 3B, 3E, and 3F). Thus, mutation of *eat-4* causes the acute response defect of *eat-4* strains.

We next sought to determine whether *eat-4* is expressed in I2 by examining transgenic worms carrying the *njEx378*[*eat-4*::*gfp*] transgene. We observed fluorescence in I2 (Figure 3C), indicating that I2 is likely glutamatergic. A recent study also observed *eat-4* expression in I2 [26]. To determine whether *eat-4* functions in I2 for the pumping response to light, we expressed *eat-4* cDNA using an I2-specific promoter [27] (*flp-15*$_{prom}$::*eat-4 cDNA*::*gfp*). I2-specific expression of *eat-4* partially rescued the acute latency and amplitude defects of *eat-4* mutants (Figures 3D–3F), whereas *eat-4* expression in I1, AWC, and AWB (*gcy-10*$_{prom}$::*eat-4 cDNA*::*gfp*) had no effect (Figure S3I).

We previously showed that mutants of *lite-1*, which encodes a gustatory receptor ortholog critical for light avoidance [18, 20], exhibit a partially defective acute response and a completely defective recovery response [16]. Strikingly, *eat-4*; *lite-1* double mutants were nearly completely defective in the pumping response to light (Figures 3G, 3I, and 3J). I2-specific *eat-4* expression partially rescued the acute pumping response defect of *eat-4*; *lite-1* mutants (Figures 3H–3J). Together, these I2-specific expression experiments suggest that I2 secretes glutamate in response to light. The partial nature of these rescues, as well as the fact that *eat-4* mutants had a more-severe acute response defect than I2-ablated worms, suggests that glutamatergic neurons in addition to I2 function in the acute response to light.

I2 also expresses several neuropeptide genes: *flp-5*; *flp-15*; *nlp-3*; and *nlp-8* [27, 28]. Mutants defective in these neuropeptide genes had a normal acute pumping response to light (Figures S4A–S4E). Moreover, mutants defective in the neuropeptide-processing enzymes *egl-3* (PC2) and *egl-21* (CPE) also had a normal acute pumping response to light (Figures S4F–S4H). *unc-31* mutants defective in dense-core vesicle release exhibited a normal acute latency in response to light, although they did exhibit a small but statistically significant defect in acute amplitude (Figure S4I). Finally, genetic ablation of I2 did not further enhance the acute defect of *eat-4* mutants, suggesting that the entirety of I2's function in acute pumping is mediated by *eat-4* (Figure S4J). Altogether, it appears unlikely that neuropeptide signaling from I2 plays a critical role in the I2-mediated acute response to light.

## The AVR-15 GluCl Glutamate Receptor Functions in Pharyngeal Muscle

Next, we sought to identify the glutamate receptor(s) that functions downstream of I2 for the acute response to light. We tested mutants of all 18 glutamate receptors and found defective acute responses in *avr-15*(*ad1051*), *avr-14*(*ad1032*), *glc-2*(*gk179*), and

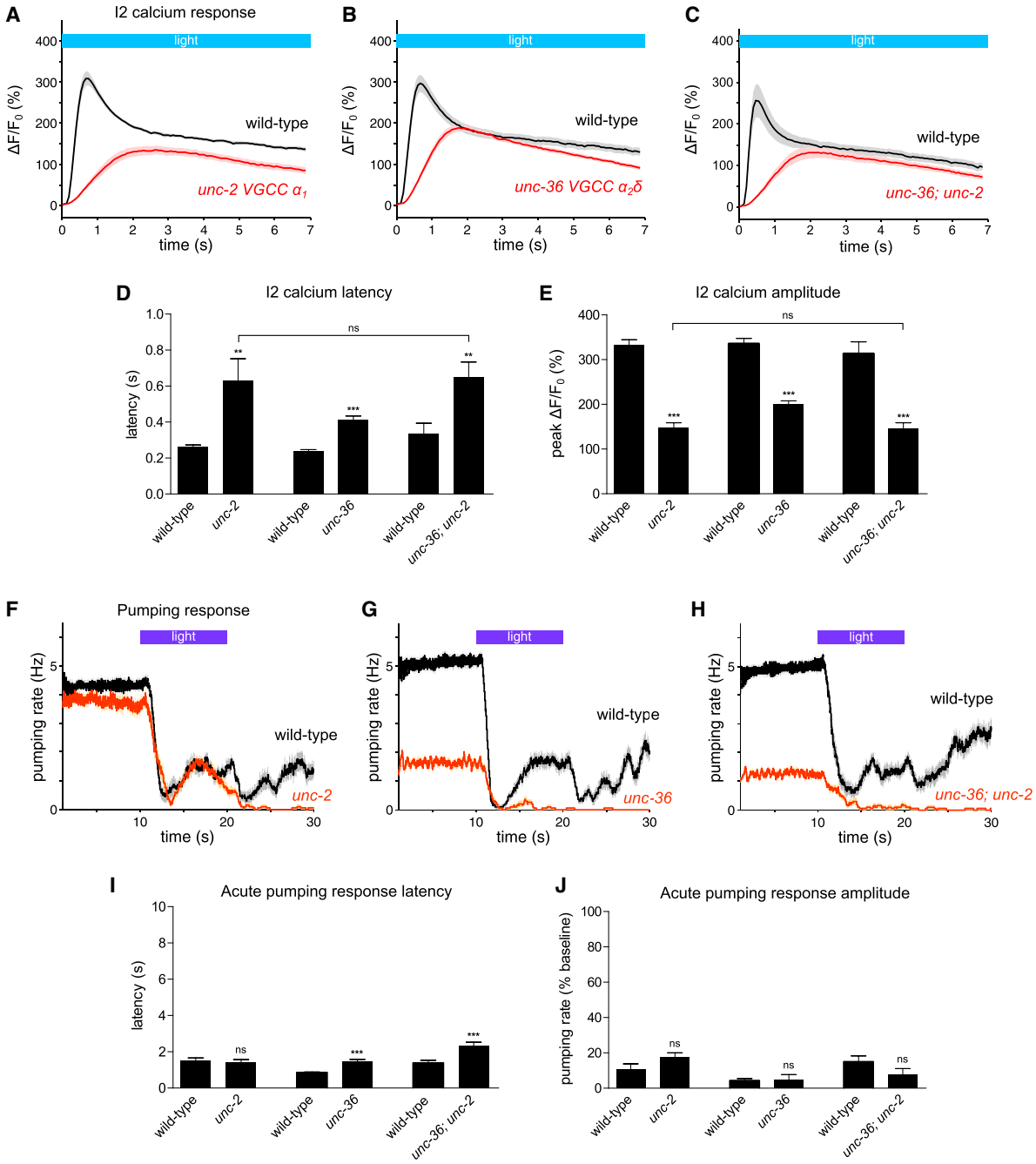


**Figure 2. The UNC-2 and UNC-36 Voltage-Gated Calcium Channels Are Partially Required for the Calcium Response of I2**

(A) *unc-2*(*e55*) mutants were partially defective in the calcium response of I2. n = 19 neurons.

(B) *unc-36*(*e251*) mutants were partially defective in the calcium response of I2. n = 19.

(C) *unc-36*; *unc-2* double mutants were not enhanced over the single mutants in their defects in the calcium response of I2. n = 21.

(D) Quantification of calcium response latency.

(E) Quantification of the peak calcium response.

(F) *unc-2* mutants showed a normal acute pumping response to light. n = 20 worms.

(G) *unc-36* mutants showed a small but significant defect in acute response latency. n = 20.

(H) *unc-36*; *unc-2* double mutants showed a small but significant defect in acute response latency. n = 20.

(I) Quantification of acute response latency, briefly defined as the time between light onset and the first missed pump.

(J) Quantification of acute response amplitude, briefly defined as the minimum of the pumping rates soon after light onset normalized to the pre-light pumping rate.

The calcium response was measured in the posterior neurite of I2. Error bars and shading around traces indicate SEM. ***$p < 0.001$; **$p < 0.01$; ns at $p < 0.05$; t test compared to corresponding wild-type or indicated strain.

See also Figure S2.

 

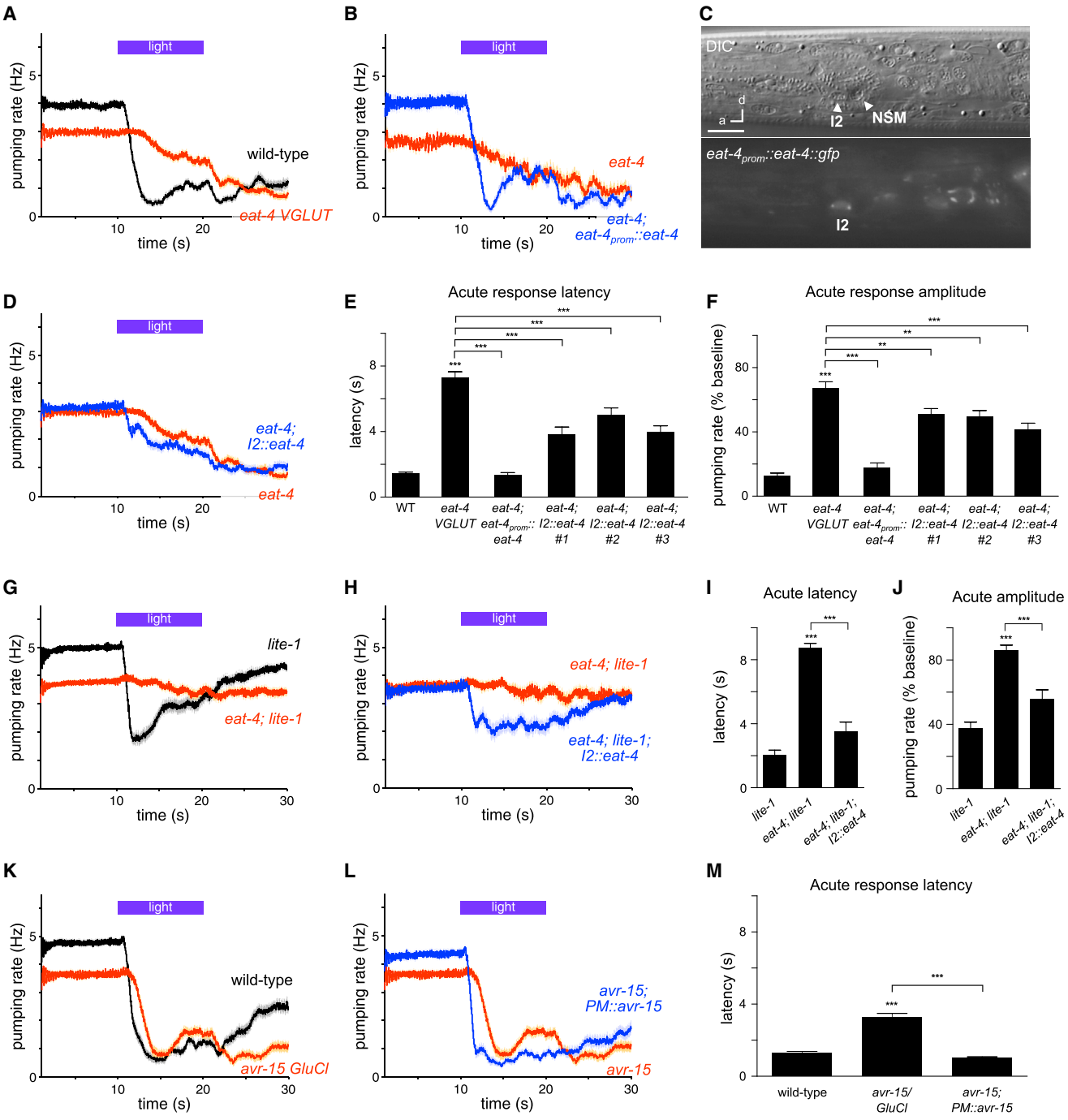


**Figure 3. The I2 Neurons Secrete Glutamate to Rapidly Block Muscle Contraction**

(A) Mutants of *eat-4*(*ky5*) *VGLUT* were defective in the acute response to light. n = 60 worms.

(B) Expression of genomic *eat-4* (*njEx378*) completely rescued the defective acute response of *eat-4* mutants. n = 20.

(C) Top: Nomarski differential interference contrast optics (DIC) image of an L4 worm head. Bottom: expression pattern of *eat-4* as indicated by a transgene carrying *njEx378*[*eat-4*$_{prom}$::*eat-4*::*gfp*]. Expression was observed in I2, but not in the NSM neuron. The scale bar represents 7 μm.

(D) I2-specific expression of the wild-type *eat-4* gene (*flp-15*$_{prom}$::*eat-4 cDNA*::*gfp*) in *eat-4* mutants partially restored the acute response to light. Three independent *eat-4* strains carrying transgenes showed a quantitative improvement in the acute response (see E and F). The trace from strain no. 1 is shown. n = 55.

(E and F) Quantifications of acute response latency (E) and acute response amplitude (F) are shown. # indicates independently integrated transgenic strains. n = 55–60.

(G) *eat-4*(*ky5*); *lite-1*(*ce314*) double mutants were nearly completely defective in the pumping response to light. The *lite-1*(*ce314*) trace includes data previously published [16]. n = 80.

(H) I2-specific expression of the wild-type *eat-4* gene in *eat-4*; *lite-1* double mutants partially restored the acute pumping response to light. n = 40.

*(legend continued on next page)*

*glc-4*(*ok212*) (Figures 3K and S5). Here, we report our detailed analysis of *avr-15*, because these mutants exhibited a defect in the latency of the acute response similar to that of I2-ablated worms (Figures 3K and 3M). *avr-15* is expressed in pharyngeal muscle [29], and we found that pharyngeal-muscle-specific expression of *avr-15* (*myo-2*$_{prom}$::*avr-15 cDNA*) fully rescued the latency defect of *avr-15* mutants (Figures 3L and 3M). This result indicates that the AVR-15 glutamate receptor functions in pharyngeal muscle to reduce the latency of the acute response to light.

## The I2 Neurons Synapse onto Pharyngeal Muscle

Our findings that I2 secretes glutamate and that the AVR-15 glutamate receptor functions in muscle suggest that I2 signals directly to muscle after being activated by light. However, the described connectome does not include any synapses from I2 to muscle but rather identifies synapses from I2 to five neuron classes (NSM, I4, I6, M1, and MC) and gap junctions with two neuron classes (M1 and I1; Figure 4A, derived from [7]). If some or all of these neurons function together as relay stations between I2 and muscle, ablating them together would be expected to cause a defect at least as severe as that caused by I2 ablation. Worms lacking all pharyngeal neurons except I2, M4, and MC (15 neurons killed per animal) did not exhibit a defect in the acute response to light (Figures 4B–4D), consistent with the hypothesis that I2 signals directly to muscle.

To further explore this possibility, we searched for additional synapses from I2 by examining the pharynx using transmission electron micrographs of serial sections (ssTEM). We identified an area as a synapse if it contained two or more synaptic or dense-core vesicles near the plasma membrane or a clearly visible presynaptic dense projection (DP) [30]. We confirmed the previous finding of synapses from I2 onto NSM, I4, and I6 and found that these synapses had an average dense projection volume of nearly 1,500,000 nm$^3$ (Figure S6). Additionally, we found 13 to 14 synapses from each I2 neuron onto pharyngeal muscle 3 (PM3) and a smaller number of synapses onto pharyngeal muscles 1 (PM1), 4 (PM4), and 5 (PM5) (Figures 4E–4H and S6). These neuromuscular synapses localized primarily to the anterior neurite of I2 and had much-smaller dense projections (average of ~80,000 nm$^3$). The presence of synapses from I2 to PM3 was confirmed in a second worm (worm no. 5; data not shown). Furthermore, when we re-examined the imagery used to generate the published connectome (the N2T series) with our criterion for identifying a synapse, we found six synapses from I2R onto PM3 and 15 synapses from I2L onto PM3. These synapses from I2 directly onto pharyngeal muscle could be the sites of I2 neurotransmission in response to light. Together, these data suggest that the I2 neurons function not only as sensory neurons but also as motor neurons to inhibit the pumping rhythm by directly silencing muscle.

## The I1 and RIP Interneurons Function in the Same Pathway in Parallel to I2

We next sought to identify additional neural circuits that could account for the acute response that remained after I2 ablation. We used laser microsurgery to kill each of the remaining 13 neuron classes in the pharynx. Although ablation of most neurons had minimal to no effect on the pumping response to light (Figure S7), we found that ablation of the I1, MC, and M1 neurons had effects.

Ablation of the I1 neuron pair impaired the acute response, as measured by both response latency and amplitude (Figures 5A, 5G, and 5H). This result indicates that I1 promotes the acute response to light.

To determine whether I1 functions in the same neural pathway as I2, we conducted double ablations with the goal of interpreting our results as double mutants are interpreted in genetic studies [31]. Double ablation of I1 and I2 caused a defect in the acute response that was more severe than either single ablation (Figures 5B, 5G, and 5H), suggesting that I1 and I2 function in parallel. To assess whether other pharyngeal neurons might also be involved, we ablated all pharyngeal neurons except I1, I2, M4, and MC. These animals retained a normal acute response to light (Figures 5C, 5G, and 5H), making it unlikely that any other pharyngeal neurons beyond I1, I2, M4, and MC play a critical role in the acute response.

We next sought neurons that might function upstream of I1. The pharyngeal nervous system is anatomically connected to the main nervous system through gap junctions between the I1 and RIP neurons [7]. Ablation of the RIP neuron pair did not affect the acute response (Figures 5D, 5G, and 5H). Because I2 ablation enhanced the defect of I1 ablation, we suspected that I2 ablation might serve as a sensitized background with which to observe more-subtle functions for neurons in the I1 circuit. Worms lacking both RIP and I2 showed a significant enhancement of the acute latency and amplitude defects of I2-ablated worms (Figures 5E, 5G, and 5H). Consistent with the hypothesis that RIP acts in the same pathway as I1, ablation of RIP and I1 together did not enhance the defect of I1-ablated animals (Figures 5F–5H). Taken together, these results suggest that RIP and I1 function in the same neural pathway in parallel to I2.

To determine whether acute physiological changes in I1 are sufficient to inhibit pumping, we manipulated the voltage of I1 using optogenetics. Worms removed from food pump at a low rate (1 to 2 Hz), and optogenetic depolarization of I1 using channelrhodopsin (ChR2) [32, 33] (*gcy-10*$_{prom}$::*chr2*::*yfp*) expressed in otherwise light-insensitive worms (*lite-1 gur*-3) [16] caused an immediate increase in the pumping rate of freely moving animals

(I) Quantification of acute response latency.
(J) Quantification of acute response amplitude.
(K) *avr-15*(*ad1051*) glutamate-gated chloride channel (*GluCl*) mutants had a delayed pumping response to light. n = 60.
(L) Pharyngeal muscle (PM)-specific expression of the wild-type *avr-15* gene (*myo-2*$_{prom}$::*avr-15A cDNA*) in *avr-15* mutants restored normal acute response latency. n = 60.
(M) Quantification of acute response latency.
Error bars and shading around traces indicate SEM. ***p < 0.001; **p < 0.001; t test compared to wild-type, *lite-1*, or indicated strain.
See also Figures S3–S5.

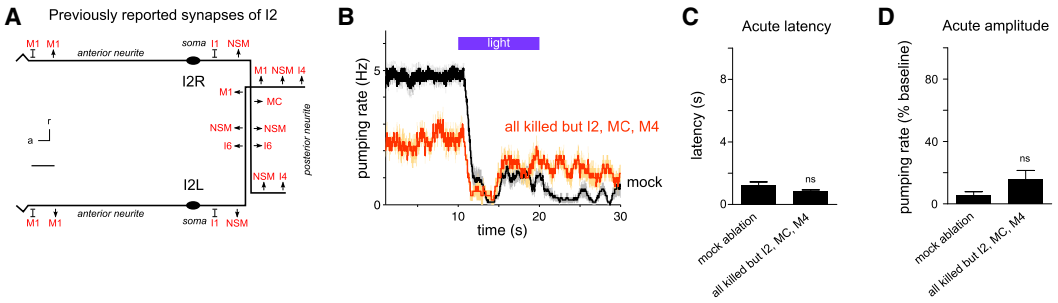


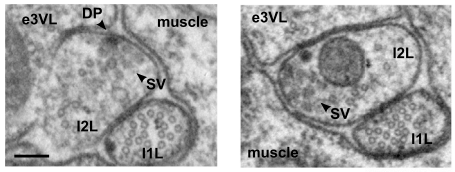


F

I2 synapses onto muscle

| | From | To | # synapses | # sections | DP vol. (nm$^3$) | vesicle area (nm$^2$) |
|---|---|---|---|---|---|---|
| anterior neurite | I2L | PM3 | 13 | 133 | 893,560 | 318,307 |
| | I2R | PM3 | 14 | 108 | 743,900 | 263,264 |
| | I2L | PM1 | 1 | 9 | 116,200 | 23,192 |
| | I2R | PM1 | 3 | 13 | 973,400 | 40,288 |
| | I2R | PM4 | 2 | 7 | 623,300 | 11,156 |
| posterior neurite | I2R | PM4 | 1 | 6 | 1,233,900 | nd |
| | I2L | PM5 | 1 | 1 | 408,600 | nd |
| | I2R | PM5 | 1 | 5 | 813,500 | nd |

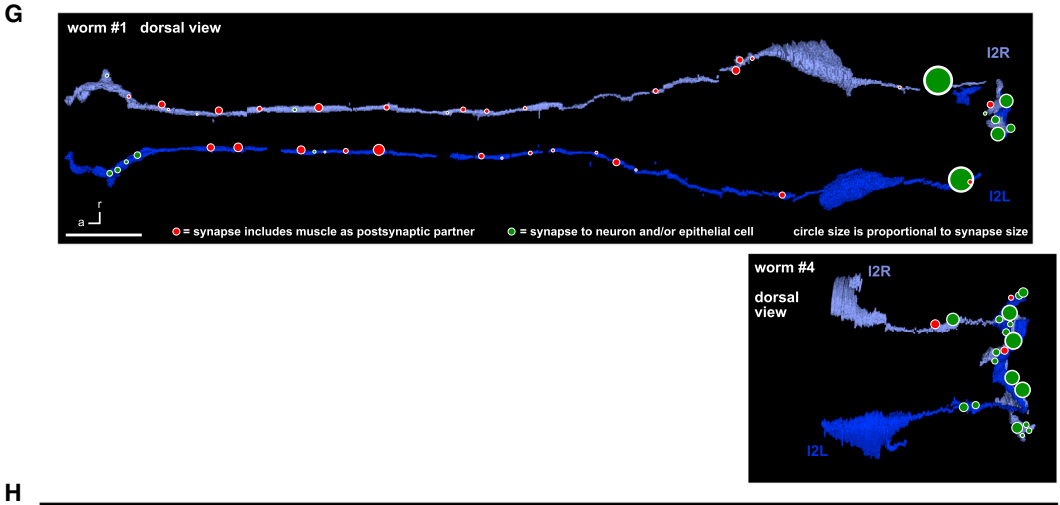


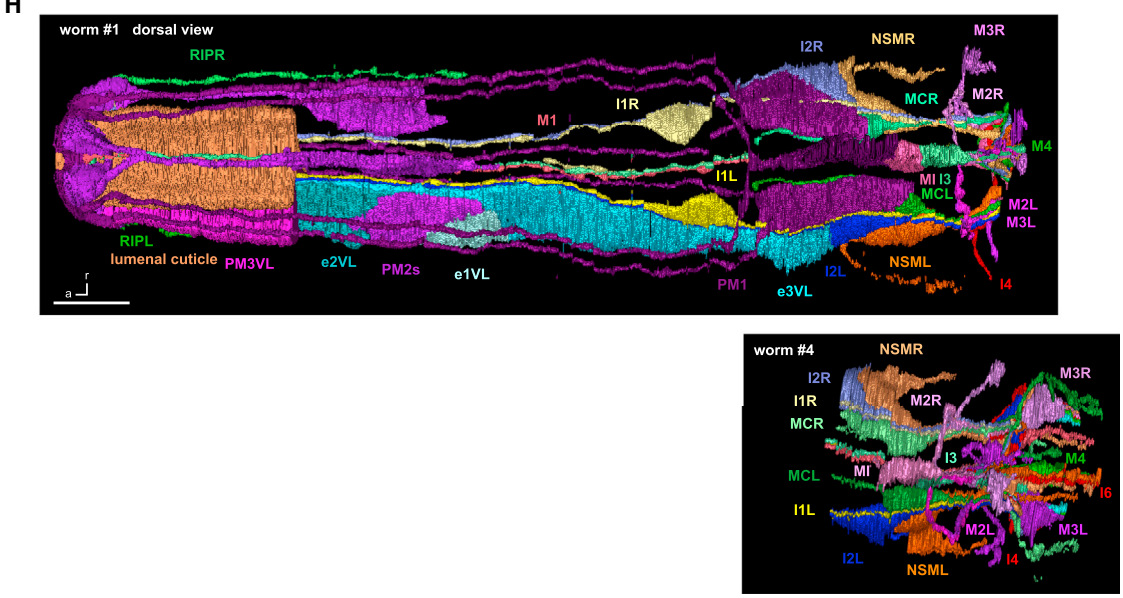


*(legend on next page)*

(Figures 5I and 5K). Because the *gcy-10* promoter drives expression in neurons in addition to I1, we confirmed that I1 was necessary for the optogenetic effect on pumping by ablating I1 and observing that ChR2 activation no longer increased pumping (Figures 5J and 5K). Reciprocally, optogenetic hyperpolarization of I1 using halorhodopsin (eNpHR3) [34] (*gcy-10*$_{prom}$::*enphr3*::*yfp*) caused an immediate decrease in pumping rate of worms on food (Figures 5L and 5N). Ablation of I1 led to loss of the optogenetic effect on pumping (Figures 5M and 5N), indicating that optogenetic inhibition of pumping required I1. Optogenetic manipulations of I1 have previously been reported to result in similar effects on the pumping of immobilized worms [15]. Although we were unable to observe changes in calcium in I1 and RIP in response to light using GCaMP3 [35] (data not shown), the effect on pumping of depolarizing and hyperpolarizing I1 suggests that light might inhibit pumping via the I1 circuit by causing hyperpolarization of I1.

## The MC Motor Neurons Function Serially with I1 and in Parallel to I2

To identify cells that function downstream of I1, we examined I1 connectivity within the pharynx. I1 synapses onto several neurons, including the pair of MC motor neurons [7]. MC-ablated worms had a modest acute response to light, although quantification could not be directly compared with that of wild-type because of the substantial reduction of baseline pumping (Figures 6A and 6D). Using logic similar to that used to identify a role for RIP, we sought evidence for a function of MC in the I1 pathway by ablating MC in the sensitized I2-ablated background. Worms lacking MC and I2 exhibited essentially no acute response to light, and the acute response latency was significantly lengthened over that of MC-ablated worms (Figures 6B and 6D). I1 ablation in addition to MC ablation did not alter the response to light of MC-ablated worms (Figures 6C and 6D). These results suggest that I1 and MC function in the same pathway and act in parallel to I2.

If MC functions downstream of I1, optogenetic depolarization of I1 might be expected to increase calcium in MC. Immobilization for calcium imaging caused worms to completely inhibit pumping, and essentially no calcium transients were observed in MC (*flp-21*$_{prom}$::*gcamp3*; *lite-1 gur-3*). Strikingly, ChR2-mediated depolarization of I1 and other *gcy-10*-expressing neurons induced pumping as well as rhythmic bursts of calcium in MC, M4, and M2 (Figures 6E–6K; Movie S1). For MC, the most substantial calcium increase occurred in the posterior ventral neurite. Hyperpolarization of *gcy-10*-expressing neurons, including I1, did not cause a calcium reduction in MC (data not shown), perhaps because MC was already inhibited by immobilization. A behavioral function of MC downstream of I1 was also recently demonstrated [15]. Altogether, these results are consistent with a model in which light hyperpolarizes I1 to inhibit MC to inhibit pumping.

## The M1 Motor Neuron Promotes Spitting of Pharyngeal Contents

In addition to the acute inhibition of pumping observed on light onset, prolonged light exposure caused a subsequent increase in pumping, which we named the "burst" response (Figure 1A). In our study of neural function by systematic ablation, we discovered that the M1 motor neuron reduced the burst response to light (Figures 7A and 7B). M1 ablation did not affect the acute response (Figures 7C and 7D), indicating that M1 is not a necessary component of the acute response circuit.

We occasionally observed bubbles emerging from the worm's mouth during the burst response (9 of 40 trials), suggesting that light might reverse the flow of material within the pharynx. To gain further insight, we used high-frame-rate videos to observe flow direction in worms ingesting mineral oil or 1-μm beads. Normal feeding pumps in the absence of shortwave light corresponded to corpus (anterior pharynx) contraction-relaxation cycles with oil or beads being sucked into the corpus and retained there (Figure 7E) [10]. We were surprised to observe that after light exposure inhibited pumping, light altered the corpus contraction-relaxation cycles, such that the oil or beads sucked into the corpus were expelled rather than retained (Figures 7F, 7G, and 7L; Movie S2). We conclude that a spitting-like response occurs during the burst response to light.

M1-ablated worms were defective in the emission of bubbles from the pharynx during light exposure (0 of 53 trials). Moreover,

**Figure 4. The I2 Neurons Synapse Directly onto Pharyngeal Muscle**

(A) Schematic of I2 synapses previously identified [7]. Arrows indicate chemical synapses; barred lines indicate gap junctions. r, right. Scale bar, 6 μm.

(B) Laser ablation of all pharyngeal neurons except I2, MC, and M4 did not affect acute response latency. n = 6 trials, 2 worms.

(C) Quantification of acute response latency.

(D) Quantification of acute response amplitude.

(E) Electron micrographs of two synapses from the anterior neurite of I2L (the left I2 neuron) to pharyngeal muscle. These synapses are dyadic and oppose an epithelial cell (e3VL) as well as muscle (PM3). The left panel displays a synapse with both a dense projection and vesicles, whereas the right panel displays a synapse with only vesicles. DP, dense projection; SV, synaptic vesicles. The scale bar represents 100 nm.

(F) Table showing measurements for synapses identified between I2 and PM. The listed DP volumes and vesicle areas are the sum of these values across all synapses with the specific partners indicated by the row in the table.

(G) Morphological reconstruction of parts of four I2 neurons in two worms. The I2 neurons in worm no. 1 were completely reconstructed except in the posterior nerve ring, which was lost. This missing area was reconstructed in worm no. 4, as well as the entire posterior neurite. Red circles indicate synapses onto muscle (including dyadic synapses in which muscle is one of the partners), and green circles indicate synapses onto neurons and occasionally onto epithelial cells. Circles are scaled to synapse size, as defined by the sum of the dense projection volume and synaptic vesicle volume. View is from the dorsal side. The scale bar represents 5 μm.

(H) Morphological reconstruction of the anterior half of the pharynx, including part of the extrapharyngeal RIP neurites. Ventral left (VL) epithelial cells and pharyngeal muscles are shown; only part of pharyngeal muscle 3 (PM3) and the lumenal cuticle are shown. Gland cells, marginal cells, and pharyngeal muscles 4 and 5 are not shown. View is from the dorsal side. The scale bar represents 5 μm.

Error bars and shading around traces indicate SEM. nd, not determined. ns at $p < 0.05$; t test compared to mock control.

See also Figure S6 for electron micrographs and quantification of all observed I2 synapses.

 

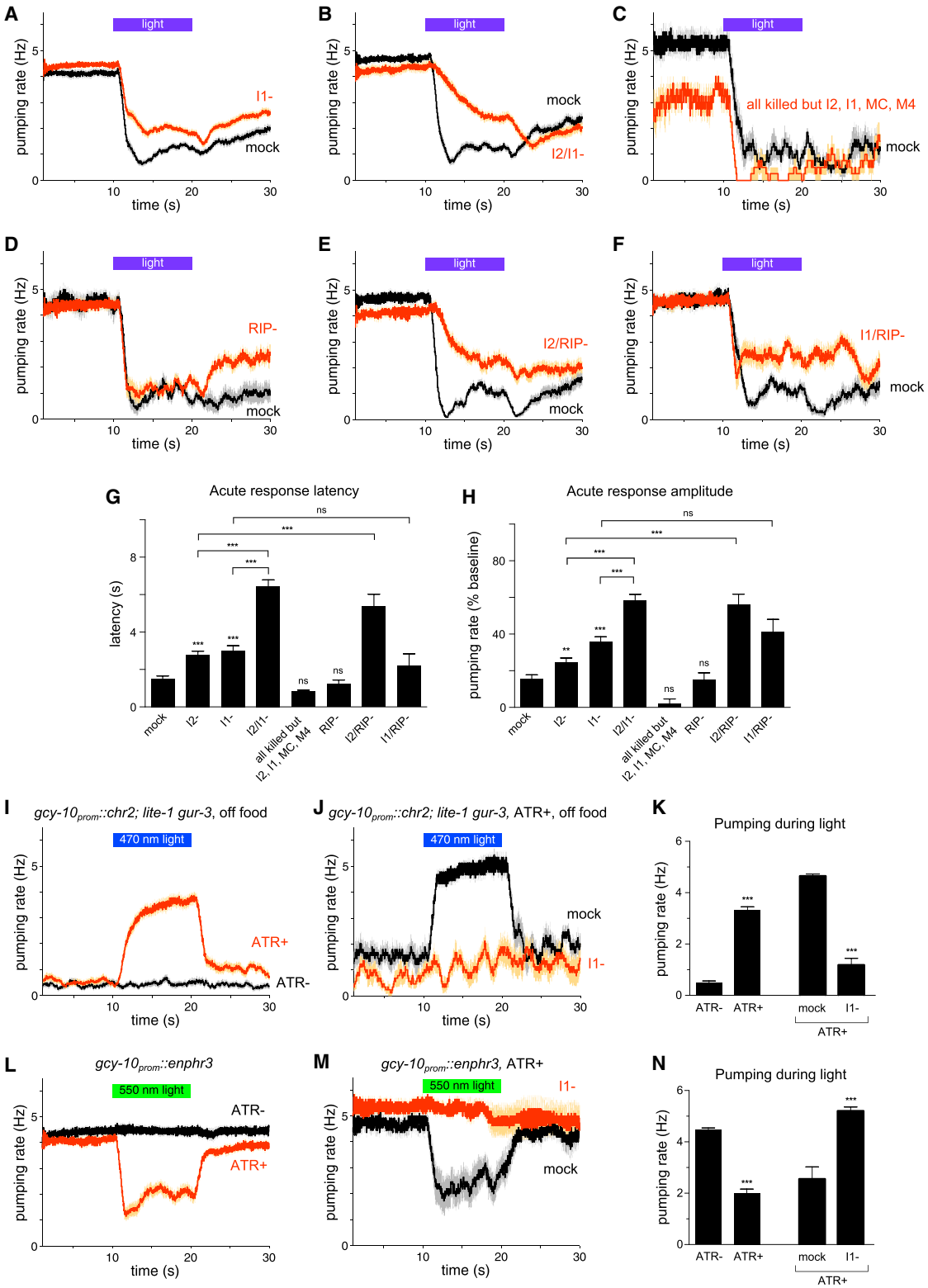


**Figure 5. The I1 and RIP Interneurons Likely Constitute a Neural Pathway that Controls Acute Inhibition in Parallel to I2**

(A) I1 ablation caused a defect in the acute response to light. n = 138 trials, 74 worms.

(B) I2/I1 double ablation enhanced the acute response defects caused by either single ablation. n = 75 trials, 25 worms.

(C) Laser ablation of all pharyngeal neurons except I2, I1, MC, and M4 did not affect the acute response. n = 4 trials, 4 worms.

*(legend continued on next page)*

M1 ablation caused a complete loss of spitting during light exposure (Figures 7H and 7L), indicating that M1 promotes spitting.

We next sought to determine whether M1 functions downstream of the acute response circuit. Ablation of I1 and I2 separately or together did not result in a loss of spitting (Figures 7I–7L), indicating that I1 and I2 do not have a necessary function upstream of M1 for spitting. These results demonstrate that the M1-defined spitting circuit can function independently of the acute inhibition circuits.

## DISCUSSION

By studying the *C. elegans* pharyngeal response to light, we have identified three neural circuits that control a myogenic muscular pump. Light rapidly inhibits rhythmic feeding, and this acute inhibition is promoted by the I2 pharyngeal neurons [16]. Here, we show that I2 is activated in the absence of neural input, suggesting that the I2 neurons function as sensory neurons. The I2 calcium response to light is partially mediated by the voltage-gated calcium channel proteins UNC-2 and UNC-36. Moreover, contrary to previous reports, our electron microscopic analysis indicates that I2 directly synapses onto pharyngeal muscle, suggesting that the I2 neurons function as motor neurons and therefore constitute a monosynaptic circuit. I2 secretes glutamate, which stimulates the AVR-15 glutamate-gated chloride channels in muscle to acutely inhibit the pumping rhythm. Additionally, we identify a second neural pathway for acute inhibition that consists of the RIP and I1 interneurons and the MC motor neurons, which act in the same pathway in parallel to I2. Optogenetic hyperpolarization of I1 inhibits pumping, suggesting that light could inhibit pumping by hyperpolarizing I1. Finally, a third pathway that includes the M1 motor neuron promotes spitting (flow reversal) during continued light exposure.

### Functional Modularity as a Principle in the Evolution of Neural Circuits

Our findings are summarized in a model (Figure 8). During normal feeding, MC promotes a high rate of pumping via innervation of marginal cells and pharyngeal muscle 4 (PM4) [7, 17]. Exposure to light causes acute inhibition of pumping via two pathways. In the first pathway, I2 detects light via the GUR-3 gustatory receptor and blocks pumping by directly inhibiting muscle. To reinforce this block, we speculate that sensory neurons outside the pharynx detect light via LITE-1 [16] and transmit a signal to RIP, RIP hyperpolarizes I1, and I1 inhibits MC, the primary driver of pumping. This pathway is inferred from laser ablation and optogenetic experiments and would be more compellingly demonstrated if corresponding physiological signals can be observed. This partially redundant strategy acts more potently to inhibit pumping than does either single pathway alone.

Remarkably, a distinct neural circuit adds a new degree of freedom to the behavioral repertoire of the pharynx. The M1 neuron causes flow reversal or ''spitting'' and does not require the I1 or I2 neurons involved in acute pumping inhibition. This modular design suggests how this neural system might have evolved, with new circuits being added in parallel to modulate an existing behavior, without compromising the effects of a previously existing neural circuit. Examination of the cell types and connectomes in related nematodes might provide further insight into the evolution of these three neural circuits. The synapses from I2 to pharyngeal muscle, as well as the gap junctions between RIP and I1, are present in the predatory nematode *Pristionchus pacificus*, but the chemical synapses from I1 to MC seem to be missing [36]. Additionally, whereas I2, RIP, I1, MC, and M1 are present in the nematode *Aphelenchus avenae*, the morphologies of RIP, I1, and I2 are altered relative to those of the corresponding neurons in *C. elegans* [37]. By studying the functional and behavioral consequences of these morphological and synaptic variations across species, the evolutionary history of these neural circuits might elucidate fundamental kinds of changes that can occur at the neural-circuit level during evolution and reveal principles that apply to a broad range of animals.

### The Challenge of Inferring Function from Structure in Connectomics

Our work highlights a challenge in using a connectome to identify a functional neural circuit. The *C. elegans* pharyngeal connectome has been available since 1976 [7]; however, this connectome, established from serial section electron micrographs from multiple animals, lacked the functional synapses that we found between I2 and muscle. One possible reason for this omission is that those authors used a stricter criterion for identifying a synapse than we used. For example, perhaps they required that

(D) RIP ablation did not affect the acute response. n = 21 trials, 6 worms.
(E) I2/RIP double ablation enhanced the acute response defect of I2 ablation. n = 26 trials, 9 worms.
(F) I1/RIP double ablation did not enhance the acute response defect of I1 ablation. n = 18 trials, 6 worms.
(G) Quantification of acute response latency.
(H) Quantification of acute response amplitude.
(I) Optogenetic depolarization of *gcy-10$_{prom}$*::*chr2*; *lite-1 gur-3* worms caused an increase in pumping rate off of food in the presence of all-*trans* retinal (ATR+), but not in its absence (ATR−). n = 50 worms.
(J) Optogenetic depolarization of *gcy-10$_{prom}$*::*chr2*; *lite-1 gur-3* worms failed to induce pumping after laser ablation of I1, indicating that the optogenetic effect requires I1. n = 9 trials, 8 worms.
(K) Quantification of the average pumping rate during 10 s of optogenetic depolarization.
(L) Optogenetic hyperpolarization of *gcy-10$_{prom}$*::*enphr3* worms caused a decrease in pumping rate on food in the presence of ATR (ATR+), but not in its absence (ATR−). n = 47 worms.
(M) Optogenetic hyperpolarization of *gcy-10$_{prom}$*::*enphr3* worms failed to inhibit pumping after laser ablation of I1, indicating that the optogenetic effect requires I1. n = 11 worms.
(N) Quantification of the average pumping rate during 10 s of optogenetic hyperpolarization.
Error bars and shading around traces indicate SEM. ***p < 0.001; **p < 0.01; ns at p < 0.05; t test compared to wild-type or as indicated.
See also Figure S7.

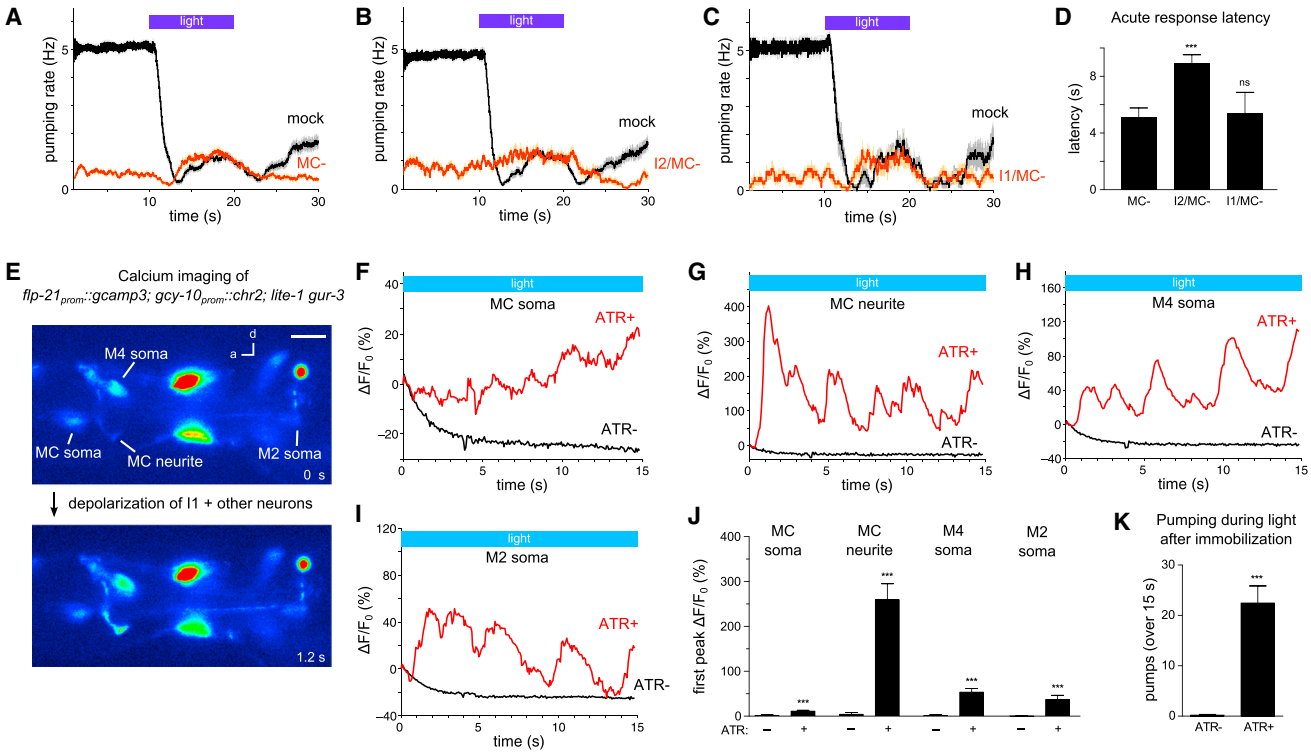


**Figure 6. The MC Neurons Likely Act in the Same Neural Pathway as I1 and in Parallel to I2**

(A) MC-ablated worms displayed a modest acute response. n = 49 trials, 20 worms.

(B) I2/MC double ablation caused a severe acute response defect. n = 17 trials, 11 worms.

(C) I1/MC double ablation did not cause a severe acute response defect. n = 9 trials, 9 worms.

(D) Quantification of acute response latency. Comparison with mock-ablated animals was not done because of the substantial difference in baseline pumping rate.

(E) An example of calcium responses observed in the MC soma, MC neurite, M4 soma, and M2 soma (*flp-21*$_{prom}$*::gcamp3*) in response to ChR2 depolarization of I1 and other *gcy-10*-expressing neurons in a *lite-1 gur-3* mutant. The scale bar represents 10 μm.

(F) Quantification of the calcium response of the MC soma shown in (E).

(G) Quantification of the calcium response of the MC neurite shown in (E).

(H) Quantification of the calcium response of the M4 soma shown in (E).

(I) Quantification of the calcium response of the M2 soma shown in (E).

(J) Quantification of the amplitude of the first calcium spike observed in each labeled compartment in response to ChR2 depolarization of I1 and other *gcy-10*-expressing neurons in *lite-1 gur-3* mutants. n ≥ 13 worms.

(K) ChR2 depolarization of I1 and other *gcy-10*-expressing neurons caused pumping by immobilized *lite-1 gur-3* worms. n ≥ 17 worms.

In (J) and (K), data were pooled across two independent transgene integrands (*nIs551* and *nIs552*). Error bars and shading around traces indicate SEM. ***p < 0.001; **p < 0.01; ns at p < 0.05; t test compared double ablations to MC single ablation; Mann-Whitney test compared ATR− to ATR+.

See also Movie S1.

both a presynaptic dense projection and a large number of vesicles be visible in the relevant micrographs. In our study, because functional rescue experiments strongly suggested a direct synaptic connection between I2 and muscle, we re-examined the connectivity using newly acquired image series. Using a more-permissive criterion to identify a synapse (either a presynaptic dense projection or two or more vesicles near the plasma membrane), we found many synapses from I2 to muscle. Our experience using an established connectome suggests that functional analyses remain a requisite step in the mapping of functional neural circuits.

## New Cellular Targets for Ivermectin

Avermectins, including ivermectin, are a potent class of anthelmintics widely used to promote both animal and human health [38]. We speculate that the molecular and cellular pathways for pumping inhibition identified here are shared with the pathways involved in the function of ivermectin, which is known to inhibit nematode pumping [39, 40]. First, the *avr-15* and *avr-14* glutamate-gated chloride channels that we have found to function in light-induced inhibition of pumping also function in ivermectin-induced inhibition of pumping [14]. Second, the I1 neurons identified here to function in light-induced inhibition of pumping also promote sensitivity to ivermectin [14]. Because I1 functions for responses to both light and ivermectin, the RIP-I1-MC neural circuit that functions in the light response might also function in the ivermectin response. These novel neurons (RIP and MC) that might function in the ivermectin effect might also define new cellular substrates for the development of novel anthelmintics. Because homologous neurons exist in

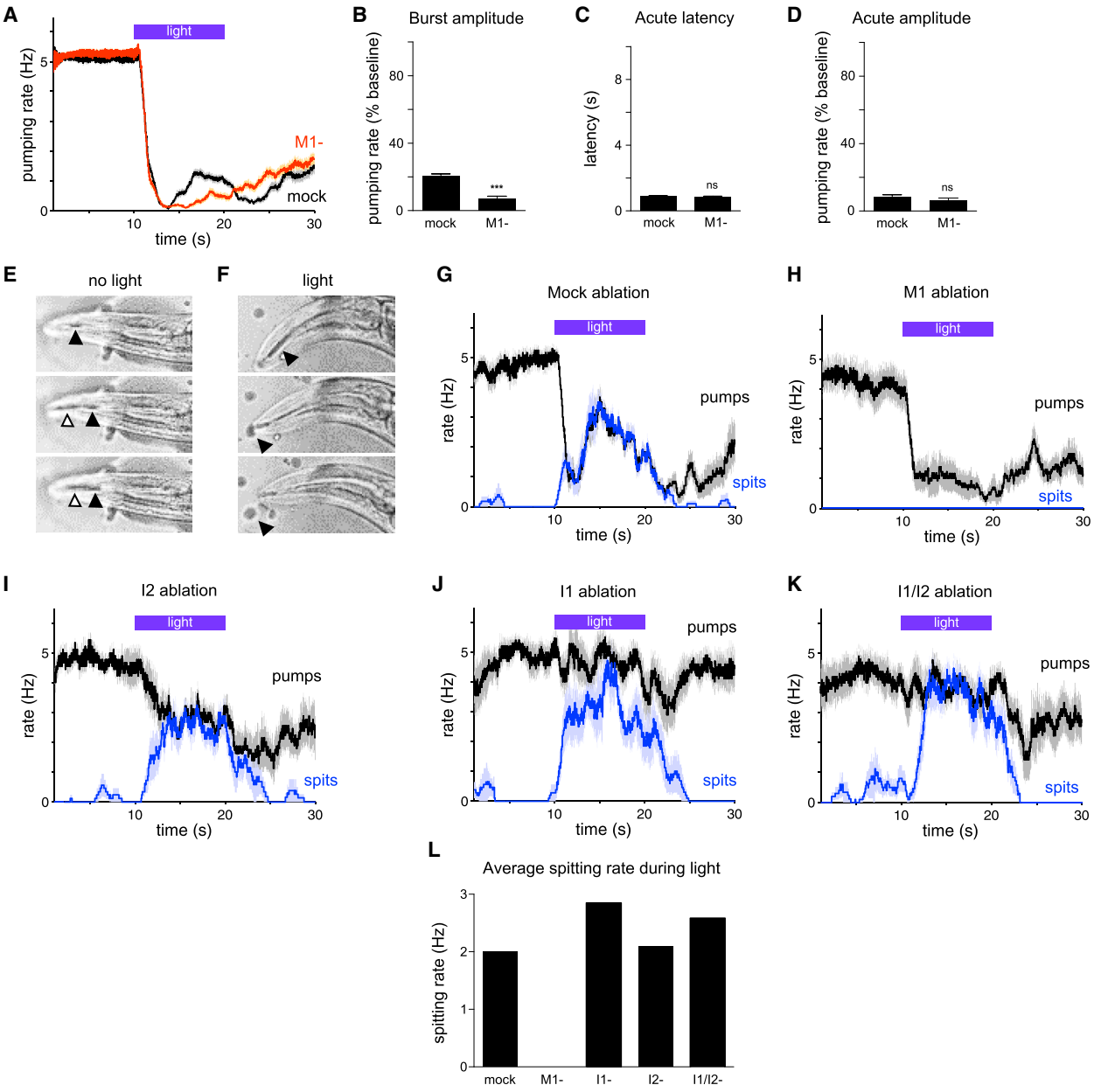


**Figure 7. The M1 Motor Neuron Promotes Spitting**

(A) M1 ablation diminished the burst response while leaving the acute response intact. n = 74 trials, 31 worms.

(B) Quantification of burst response amplitude.

(C) Quantification of acute response latency.

(D) Quantification of acute response amplitude.

(E) Image sequence showing one normal feeding pump before the worm was illuminated with light. The black arrow indicates oil that was present before the pump began, and the white arrow indicates oil that was sucked in from the environment during the pump. After completion of the pump, oil was retained in the pharynx.

(F) Image sequence showing one spitting pump that occurred during illumination with light. The black arrow indicates oil that was present before the pump began that is expelled from the pharynx after completion of the pump.

(G) For mock-ablated worms, pumps during light exposure correspond to spitting, as assayed with 1-μm beads. A "spit" was scored if beads were released from the corpus into the environment or if beads ingested during corpus contraction were not retained after corpus relaxation. n = 13 worms.

(H) For M1-ablated worms, pumping is reduced during light exposure relative to mock ablation and no spitting occurs. n = 13.

(I) For I2-ablated worms, pumping is increased during light exposure relative to mock ablation and spitting still occurs. n = 9.

(J) For I1-ablated worms, pumping is increased during light exposure relative to mock ablation and spitting still occurs. n = 11.

(K) For I1/I2 double-ablated worms, pumping is increased during light exposure relative to mock ablation and spitting still occurs. n = 10.

(L) Quantification of average spitting rate during light exposure.

In (G)–(L), assays were done with 1-μm beads. Error bars and shading around traces indicate SEM. ***$p < 0.001$; ns at $p < 0.05$; t test compared to mock control. See also Movie S2.

 

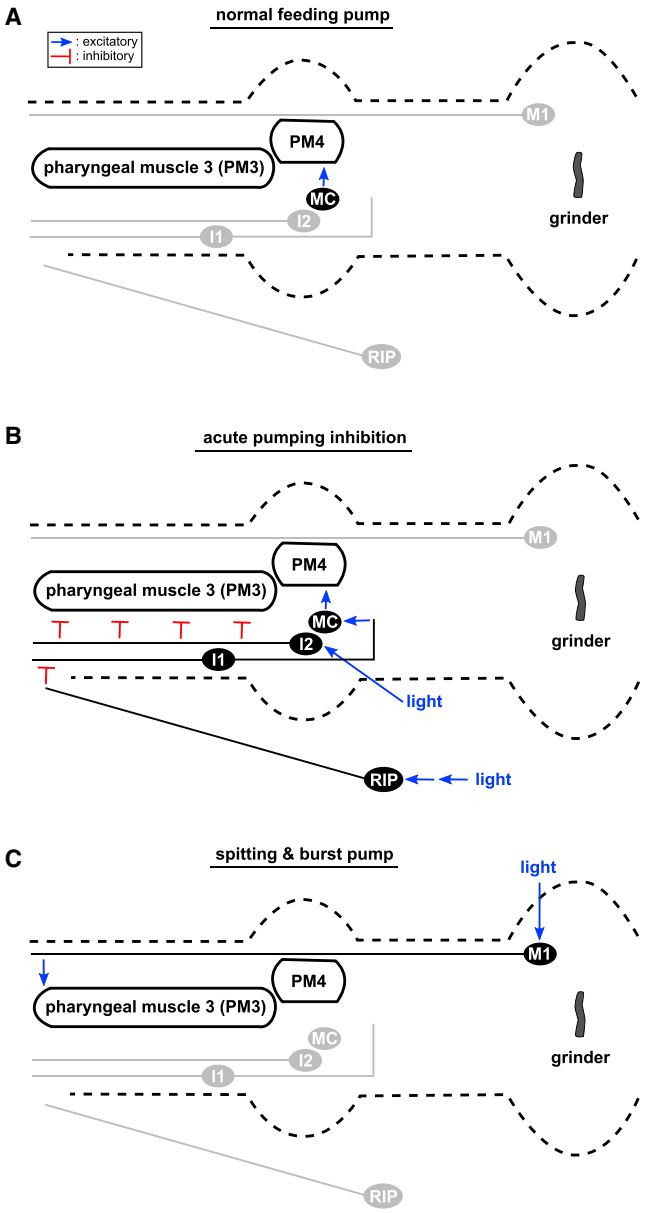


**Figure 8. Neural Circuit Control of Rhythm Inhibition and Spitting by the Myogenic Pharynx**

An expanded view of the pharynx with neurons and neurites depicted in their anatomical locations. Blue lines indicate functional activation, and red lines indicate functional inhibition. For each behavior, active neurons and neurites are in black and inactive neurons and neurites are in gray. The acute inhibition pathways are anatomically bilaterally symmetric; only one side is shown.

(A) During a normal feeding pump that occurs in the absence of shortwave light, the MC motor neurons drive muscle contractions via direct synapses onto pharyngeal muscle 4 (PM4) and marginal cells (not shown).

(B) When the worm is exposed to light, pumping is acutely inhibited via two pathways. In the first, intrinsic pathway, light directly activates the I2 sensorimotor neurons to directly inhibit PM3. In the second, extrinsic pathway, light is detected outside the pharynx and its signal is propagated via the non-pharyngeal RIP interneurons and the pharyngeal I1 interneurons to block MC function. The double arrow from light to RIP indicates that additional neurons are likely to sense light and relay the signal to RIP.

(C) When the worm is exposed to prolonged periods of light, pumping increases (the burst response) and spitting occurs via a neural pathway requiring the M1 motor neuron. We speculate that M1 is directly activated by light, because M1 expresses the light-sensitive gustatory receptor LITE-1 [16].

other nematodes [36, 37], molecular processes within these neurons could serve as targets for future drug discovery.

## Valve Control by the M1 Neuron

As we describe elsewhere [16], we believe that the pumping response to light is caused by reactive oxygen species, such as hydrogen peroxide, which can be generated by light. The worm likely senses that it is ingesting toxic material and responds by inhibiting feeding and promoting spitting using the neural circuits identified here. M1 likely functions as a sensory neuron for reactive oxygen species, because M1 expresses LITE-1 [16]. How might M1 reverse flow in the pharynx to induce spitting? During normal feeding, the anterior tip of pharyngeal muscle closes when the corpus relaxes, retaining particulates such as bacteria [10]. We speculate that, because M1 makes neuromuscular synapses at the anterior tip [7], activation of M1 could result in sustained contraction of these muscles and hold the anterior valve open. The corpus contraction-relaxation cycle would no longer retain particulates that were sucked into the corpus but instead spit them out, resulting in rinsing of the corpus. Agriculturally significant entomopathogenic nematodes regurgitate bacteria to infect their insect hosts [41], and we speculate that the M1 neuron might also function in this regurgitation.

The spitting caused by M1 is reminiscent of valvular heart disease, a pathological condition in which blood flows in the opposite direction within the heart [42]. Whereas the leading causes of valvular heart disease include valve degeneration and endocarditis, our work suggests the possibility of a novel mechanism. Specifically, in valvular heart disease, valve closure might be inhibited by intrinsic neurons that detect stimuli in the bloodstream, such as dissolved gases, metabolites, or hormones. Such a neural mechanism would be similar to how we propose the *C. elegans* M1 neuron detects reactive oxygen species to inhibit valve closure and induce spitting. If this analogy is confirmed, novel therapeutics might provide an alternative to surgery to remedy valvular heart disease by inhibiting the function of such neurons.

Additional questions remain regarding the I1 circuit. First, I1 appears to play a more-significant role than RIP in the acute light response (Figures 5A and 5D) and therefore likely has inputs in addition to RIP. Second, the physiological mechanism by which RIP, I1, and MC inhibit pumping remains uncertain. Although hyperpolarization of I1 is sufficient to inhibit pumping, whether light results in hyperpolarization of RIP, I1, and MC awaits further investigation.

In short, our studies have established that three neural circuits alter the autonomous rhythm and dynamics of a myogenic muscular pump, the *C. elegans* pharynx. Future work using physiological imaging, ablations, and neural activation and silencing will use this foundation to clarify precisely how the signal is transformed as it is relayed from neuron to neuron within each circuit. The *C. elegans* pharynx and the mammalian heart share molecular and functional features [43]. We suggest that the cellular level understanding of the modulatory neural system

we describe for the *C. elegans* pharynx will provide insight into other neural systems that control myogenic muscle organs, such as the neural circuits that modulate heart function.

## EXPERIMENTAL PROCEDURES

Experimental Procedures are available in the Supplemental Information. Custom MATLAB programs used in this study are available at http://www.wormweb.org. Electron microscopy datasets are available at http://www.openconnecto.me/catmaid/.

## SUPPLEMENTAL INFORMATION

Supplemental Information includes Supplemental Experimental Procedures, seven figures, and two movies and can be found with this article online at http://dx.doi.org/10.1016/j.cub.2015.06.052.

## AUTHOR CONTRIBUTIONS

N.B. and S.R.S. designed and conducted experiments and analyzed data; R.D. conducted electron microscopy; A.H. conducted experiments; H.R.H. designed experiments and supervised; and N.B., R.D., S.R.S., and H.R.H. wrote the manuscript.

## ACKNOWLEDGMENTS

We thank N. An, T. Hirose, D. Ma, I. Mori, R. Ketting, P. Brockie, V. Maricq, J. Dent, O. Hobert, L. Avery, S. Mitani, K. Deisseroth, the *Caenorhabditis* Genetics Center, and Addgene for strains and reagents; N. Ringstad, S. Nakano, D. Ma, N. Paquin, C. Engert, S. Luo, K. Boulias, S. Cook, and L. Avery for discussions and advice; E. Hartweig for electron microscopy assistance; D. Hall for digitized EM imagery; and R. Loya, K. Boulias, M. Fee, T. Littleton, and W. Quinn for review of the manuscript. N.B. was supported by a National Science Foundation Graduate Research Fellowship. This work was supported by NIH grant GM24663 to H.R.H. H.R.H. is an investigator of the Howard Hughes Medical Institute.

Received: February 9, 2015
Revised: May 28, 2015
Accepted: June 19, 2015
Published: July 23, 2015

## REFERENCES

1. Irisawa, H., Brown, H.F., and Giles, W. (1993). Cardiac pacemaking in the sinoatrial node. Physiol. Rev. *73*, 197–227.
2. Donnelly, G., Jackson, T.D., Ambrous, K., Ye, J., Safdar, A., Farraway, L., and Huizinga, J.D. (2001). The myogenic component in distention-induced peristalsis in the guinea pig small intestine. Am. J. Physiol. Gastrointest. Liver Physiol. *280*, G491–G500.
3. Palma, J.-A., and Benarroch, E.E. (2014). Neural control of the heart: recent concepts and clinical correlations. Neurology *83*, 261–271.
4. Chalfie, M., Sulston, J.E., White, J.G., Southgate, E., Thomson, J.N., and Brenner, S. (1985). The neural circuit for touch sensitivity in *Caenorhabditis elegans*. J. Neurosci. *5*, 956–964.
5. Chalasani, S.H., Chronis, N., Tsunozaki, M., Gray, J.M., Ramot, D., Goodman, M.B., and Bargmann, C.I. (2007). Dissecting a circuit for olfactory behaviour in *Caenorhabditis elegans*. Nature *450*, 63–70.
6. Olsen, S.R., and Wilson, R.I. (2008). Cracking neural circuits in a tiny brain: new approaches for understanding the neural circuitry of *Drosophila*. Trends Neurosci. *31*, 512–520.
7. Albertson, D.G., and Thomson, J.N. (1976). The pharynx of *Caenorhabditis elegans*. Philos. Trans. R. Soc. Lond. B Biol. Sci. *275*, 299–325.
8. White, J.G., Southgate, E., Thomson, J.N., and Brenner, S. (1986). The structure of the nervous system of the nematode *Caenorhabditis elegans*. Philos. Trans. R. Soc. Lond. B Biol. Sci. *314*, 1–340.
9. Bhatla, N. (2011). WormWeb.org: *C. elegans* interactive neural network. http://wormweb.org/neuralnet.
10. Fang-Yen, C., Avery, L., and Samuel, A.D.T. (2009). Two size-selective mechanisms specifically trap bacteria-sized food particles in *Caenorhabditis elegans*. Proc. Natl. Acad. Sci. USA *106*, 20093–20096.
11. Avery, L., and Horvitz, H.R. (1989). Pharyngeal pumping continues after laser killing of the pharyngeal nervous system of *C. elegans*. Neuron *3*, 473–485.
12. Avery, L., and Horvitz, H.R. (1987). A cell that dies during wild-type *C. elegans* development can function as a neuron in a *ced-3* mutant. Cell *51*, 1071–1078.
13. Avery, L. (1993). Motor neuron M3 controls pharyngeal muscle relaxation timing in *Caenorhabditis elegans*. J. Exp. Biol. *175*, 283–297.
14. Dent, J.A., Smith, M.M., Vassilatis, D.K., and Avery, L. (2000). The genetics of ivermectin resistance in *Caenorhabditis elegans*. Proc. Natl. Acad. Sci. USA *97*, 2674–2679.
15. Trojanowski, N.F., Padovan-Merhar, O., Raizen, D.M., and Fang-Yen, C. (2014). Neural and genetic degeneracy underlies *Caenorhabditis elegans* feeding behavior. J. Neurophysiol. *112*, 951–961.
16. Bhatla, N., and Horvitz, H.R. (2015). Light and hydrogen peroxide inhibit *C. elegans* Feeding through gustatory receptor orthologs and pharyngeal neurons. Neuron *85*, 804–818.
17. Raizen, D.M., Lee, R.Y., and Avery, L. (1995). Interacting genes required for pharyngeal excitation by motor neuron MC in *Caenorhabditis elegans*. Genetics *141*, 1365–1382.
18. Edwards, S.L., Charlie, N.K., Milfort, M.C., Brown, B.S., Gravlin, C.N., Knecht, J.E., and Miller, K.G. (2008). A novel molecular solution for ultraviolet light detection in *Caenorhabditis elegans*. PLoS Biol. *6*, e198.
19. Ward, A., Liu, J., Feng, Z., and Xu, X.Z.S. (2008). Light-sensitive neurons and channels mediate phototaxis in *C. elegans*. Nat. Neurosci. *11*, 916–922.
20. Liu, J., Ward, A., Gao, J., Dong, Y., Nishio, N., Inada, H., Kang, L., Yu, Y., Ma, D., Xu, T., et al. (2010). *C. elegans* phototransduction requires a G protein-dependent cGMP pathway and a taste receptor homolog. Nat. Neurosci. *13*, 715–722.
21. Speese, S., Petrie, M., Schuske, K., Ailion, M., Ann, K., Iwasaki, K., Jorgensen, E.M., and Martin, T.F.J. (2007). UNC-31 (CAPS) is required for dense-core vesicle but not synaptic vesicle exocytosis in *Caenorhabditis elegans*. J. Neurosci. *27*, 6150–6162.
22. Mathews, E.A., García, E., Santi, C.M., Mullen, G.P., Thacker, C., Moerman, D.G., and Snutch, T.P. (2003). Critical residues of the *Caenorhabditis elegans unc-2* voltage-gated calcium channel that affect behavioral and physiological properties. J. Neurosci. *23*, 6537–6545.
23. Schafer, W.R., Sanchez, B.M., and Kenyon, C.J. (1996). Genes affecting sensitivity to serotonin in *Caenorhabditis elegans*. Genetics *143*, 1219–1230.
24. Lee, R.Y.N., Sawin, E.R., Chalfie, M., Horvitz, H.R., and Avery, L. (1999). EAT-4, a homolog of a mammalian sodium-dependent inorganic phosphate cotransporter, is necessary for glutamatergic neurotransmission in *Caenorhabditis elegans*. J. Neurosci. *19*, 159–167.
25. Ohnishi, N., Kuhara, A., Nakamura, F., Okochi, Y., and Mori, I. (2011). Bidirectional regulation of thermotaxis by glutamate transmissions in *Caenorhabditis elegans*. EMBO J. *30*, 1376–1388.
26. Serrano-Saiz, E., Poole, R.J., Felton, T., Zhang, F., De La Cruz, E.D., and Hobert, O. (2013). Modular control of glutamatergic neuronal identity in *C. elegans* by distinct homeodomain proteins. Cell *155*, 659–673.
27. Kim, K., and Li, C. (2004). Expression and regulation of an FMRFamide-related neuropeptide gene family in *Caenorhabditis elegans*. J. Comp. Neurol. *475*, 540–550.
28. Nathoo, A.N., Moeller, R.A., Westlund, B.A., and Hart, A.C. (2001). Identification of neuropeptide-like protein gene families in *Caenorhabditiselegans* and other species. Proc. Natl. Acad. Sci. USA *98*, 14000–14005.

 

29. Dent, J.A., Davis, M.W., and Avery, L. (1997). *avr-15* encodes a chloride channel subunit that mediates inhibitory glutamatergic neurotransmission and ivermectin sensitivity in *Caenorhabditis elegans*. EMBO J. *16*, 5867–5879.

30. Stigloher, C., Zhan, H., Zhen, M., Richmond, J., and Bessereau, J.-L. (2011). The presynaptic dense projection of the *Caenorhabditis elegans* cholinergic neuromuscular junction localizes synaptic vesicles at the active zone through SYD-2/liprin and UNC-10/RIM-dependent interactions. J. Neurosci. *31*, 4388–4396.

31. Avery, L., and Wasserman, S. (1992). Ordering gene function: the interpretation of epistasis in regulatory hierarchies. Trends Genet. *8*, 312–316.

32. Nagel, G., Szellas, T., Huhn, W., Kateriya, S., Adeishvili, N., Berthold, P., Ollig, D., Hegemann, P., and Bamberg, E. (2003). Channelrhodopsin-2, a directly light-gated cation-selective membrane channel. Proc. Natl. Acad. Sci. USA *100*, 13940–13945.

33. Boyden, E.S., Zhang, F., Bamberg, E., Nagel, G., and Deisseroth, K. (2005). Millisecond-timescale, genetically targeted optical control of neural activity. Nat. Neurosci. *8*, 1263–1268.

34. Gradinaru, V., Zhang, F., Ramakrishnan, C., Mattis, J., Prakash, R., Diester, I., Goshen, I., Thompson, K.R., and Deisseroth, K. (2010). Molecular and cellular approaches for diversifying and extending optogenetics. Cell *141*, 154–165.

35. Tian, L., Hires, S.A., Mao, T., Huber, D., Chiappe, M.E., Chalasani, S.H., Petreanu, L., Akerboom, J., McKinney, S.A., Schreiter, E.R., et al. (2009). Imaging neural activity in worms, flies and mice with improved GCaMP calcium indicators. Nat. Methods *6*, 875–881.

36. Bumbarger, D.J., Riebesell, M., Rödelsperger, C., and Sommer, R.J. (2013). System-wide rewiring underlies behavioral differences in predatory and bacterial-feeding nematodes. Cell *152*, 109–119.

37. Ragsdale, E.J., Ngo, P.T., Crum, J., Ellisman, M.H., and Baldwin, J.G. (2011). Reconstruction of the pharyngeal corpus of *Aphelenchus avenae* (Nematoda: Tylenchomorpha), with implications for phylogenetic congruence. Zool. J. Linn. Soc. *161*, 1–30.

38. Cordes, E.H. (2014). Avermectins: molecules of life battle parasites. In Hallelujah Moments: Tales of Drug Discovery (New York: Oxford University Press), pp. 165–181.

39. Bottjer, K.P., and Bone, L.W. (1985). Trichostrongylus colubriformis: effect of anthelmintics on ingestion and oviposition. Int. J. Parasitol. *15*, 501–503.

40. Avery, L., and Horvitz, H.R. (1990). Effects of starvation and neuroactive drugs on feeding in *Caenorhabditis elegans*. J. Exp. Zool. *253*, 263–270.

41. Ciche, T. (2007). The biology and genome of *Heterorhabditis bacteriophora*. (WormBook), pp. 1–9.

42. Iung, B., and Vahanian, A. (2014). Epidemiology of acquired valvular heart disease. Can. J. Cardiol. *30*, 962–970.

43. Mango, S.E. (2007). The *C. elegans* pharynx: a model for organogenesis. (WormBook), pp. 1–26.

**Current Biology**

**Supplemental Information**

# Distinct Neural Circuits Control Rhythm Inhibition and Spitting by the Myogenic Pharynx of *C. elegans*

**Nikhil Bhatla, Rita Droste, Steven R. Sando, Anne Huang, and H. Robert Horvitz**

## SUPPLEMENTAL FIGURES

### Figure S1:

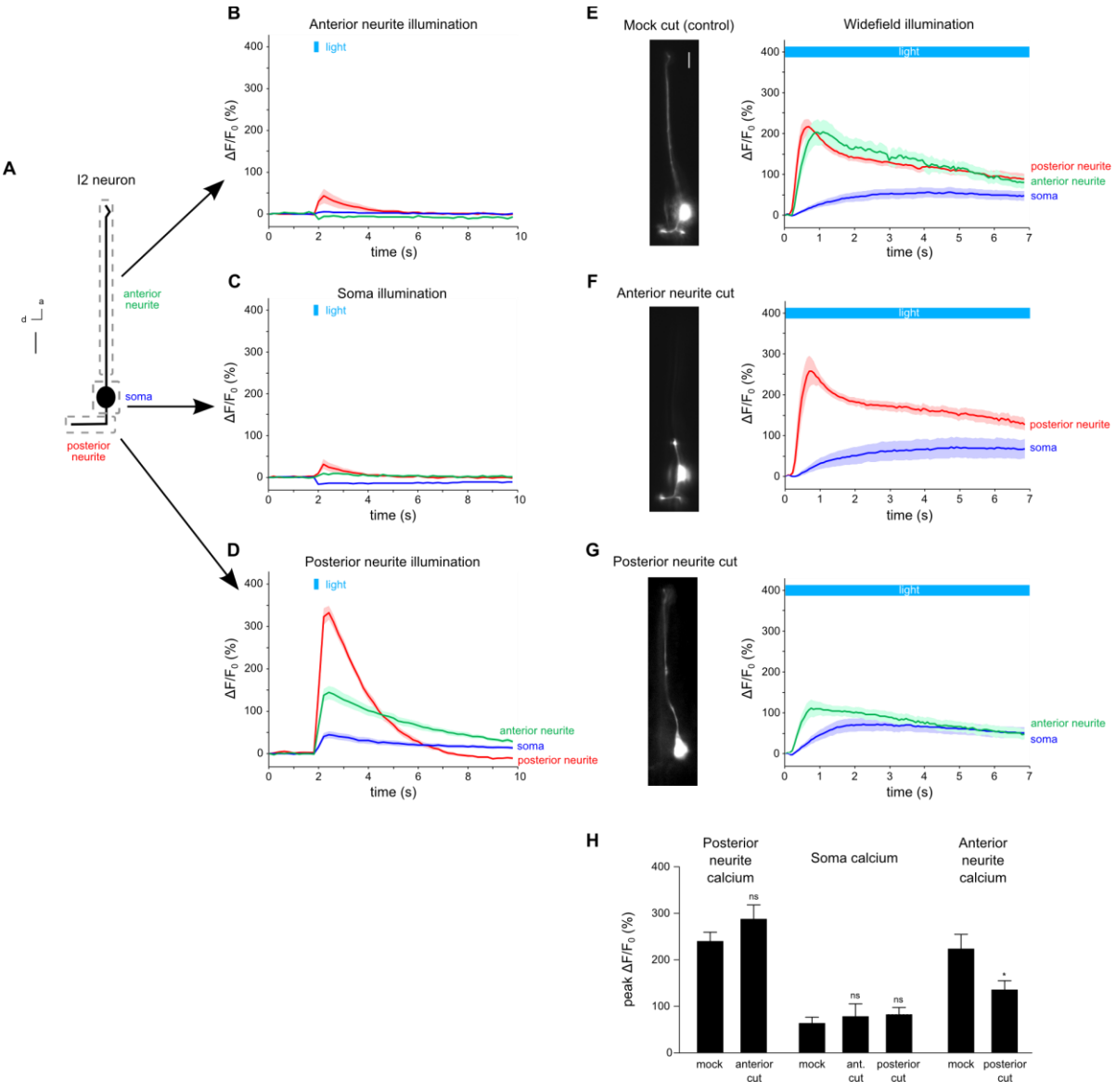


**Figure S1, related to Figure 1. Exposing different compartments of I2 to light differentially triggers a calcium response.**

(A) Diagram of an I2 neuron indicating regions exposed to spatially-restricted illumination (rastered 488 nm). Dashed gray boxes indicate three areas of illumination. d = dorsal, a = anterior, scale bar = 5 µm.
(B-G) Red trace is the response of the posterior neurite, blue is the response of the soma, and green is the response of the anterior neurite of I2.
(B) I2 responded weakly after anterior neurite illumination. n = 11 neurons.

(C) I2 responded weakly after soma illumination. n = 11.
(D) I2 responded strongly after posterior neurite illumination. n = 11. The small declines in signal in (B**)** and (C) were a consequence of anterior neurite and soma bleaching, respectively.
(E) An intact I2 neuron responded normally to light (control). n = 13.
(F) An I2 neuron with a cut anterior neurite responded normally to light. n = 7.
(G) An I2 neuron with a cut posterior neurite responded less to light than did an intact I2 neuron. n = 15.
(H) Quantification of the calcium response in different compartments after ablating the anterior or posterior neurite. Cutting the posterior neurite reduced the response in the anterior neurite but did not eliminate it.

Error bars and shading around traces indicate s.e.m. * $p < 0.05$, ns = not significant at $p < 0.05$, t-test compared to mock control.

## Figure S2:

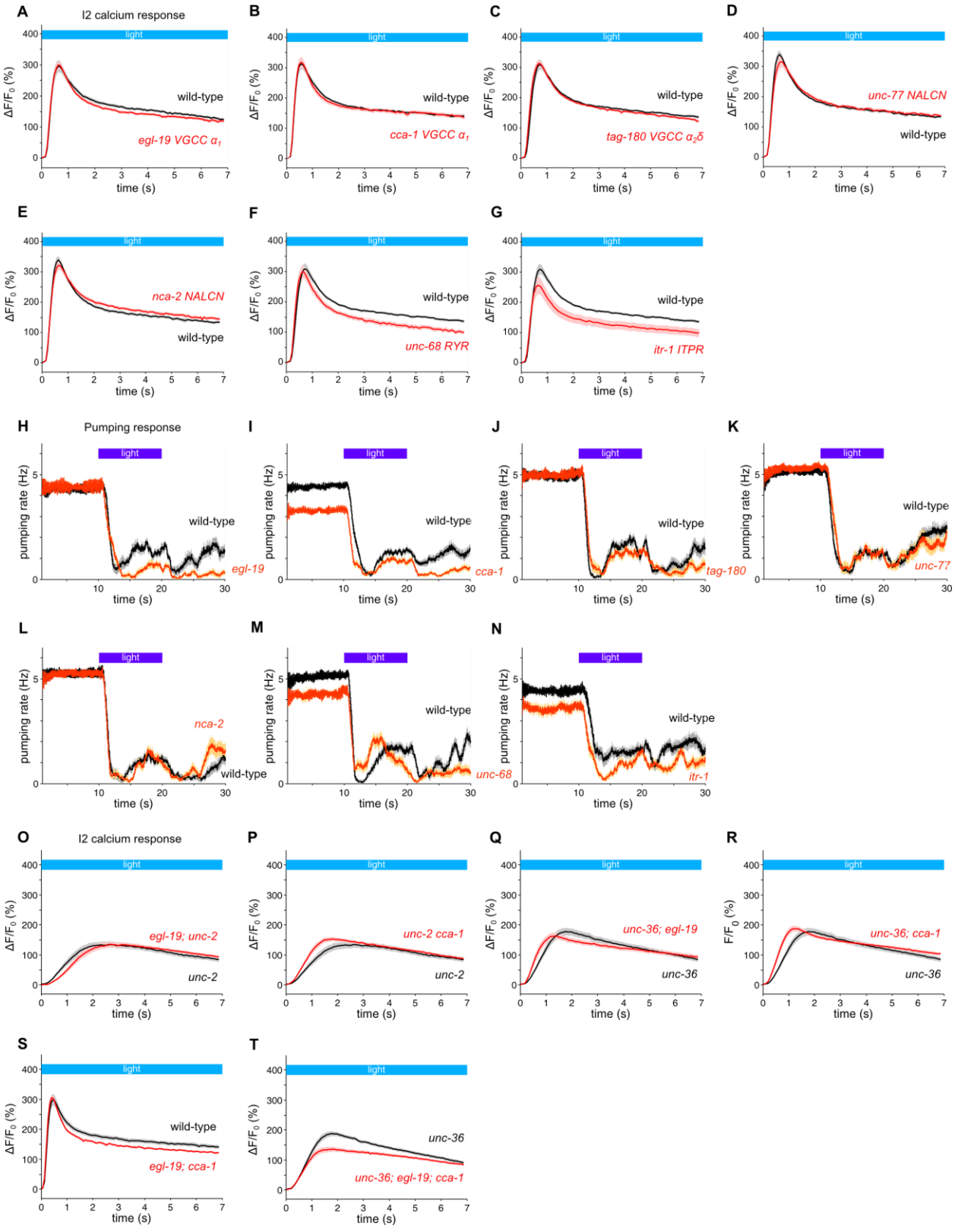
A
I2 calcium response
light
wild-type
egl-19 VGCC α1
ΔF/F0 (%)
time (s)
B
cca-1 VGCC α1
C
tag-180 VGCC α2δ
D
unc-77 NALCN
E
nca-2 NALCN
F
unc-68 RYR
G
itr-1 ITPR
H
Pumping response
pumping rate (Hz)
egl-19
I
cca-1
J
tag-180
K
unc-77
L
nca-2
M
unc-68
N
itr-1
O
egl-19; unc-2
unc-2
P
unc-2 cca-1
Q
unc-36; egl-19
unc-36
R
F/F0 (%)
unc-36; cca-1
S
egl-19; cca-1
T
unc-36; egl-19; cca-1

**Figure S2, related to Figure 2. Calcium channel mutants that exhibited a normal I2 calcium response to light, a normal acute pumping response, and a failure to enhance the I2 response defect of *unc-2* and *unc-36* mutants.**

(A) *egl-19(n582)* mutants showed a normal calcium response in I2. n = 20 neurons.
(B) *cca-1(ad1650)* mutants showed a normal calcium response in I2. n = 21.
(C) *tag-180(ok779)* mutants showed a normal calcium response in I2. n = 21.
(D) *unc-77(gk9)* mutants showed a normal calcium response in I2. n = 22.
(E) *nca-2(gk5)* mutants showed a normal calcium response in I2. n = 22.
(F) *unc-68(e540)* mutants showed a normal calcium response in I2. n = 22.
(G) *itr-1(sa73)* mutants showed a normal calcium response in I2. n = 21.

(H) *egl-19(n582)* mutants showed a normal acute pumping response to light. n = 20 worms.
(I) *cca-1(ad1650)* mutants showed a normal acute pumping response to light. n = 40.
(J) *tag-180(ok779)* mutants showed a normal acute pumping response to light. n = 20.
(K) *unc-77(gk9)* mutants showed a normal acute pumping response to light. n = 20.
(L) *nca-2(gk5)* mutants showed a normal acute pumping response to light. n = 20.
(M) *unc-68(e540)* mutants exhibited normal acute response latency but were defective in acute response amplitude ($p < 0.001$, t-test). n = 20.
(N) *itr-1(sa73)* mutants were not defective in the acute pumping response to light. n = 20.

(O) *egl-19; unc-2* double mutants showed a calcium response in I2 no more defective than *unc-2* mutants. n = 20 neurons.
(P) *unc-2 cca-1* double mutants showed a calcium response in I2 no more defective than *unc-2* mutants. n = 27.
(Q) *unc-36; egl-19* double mutants showed a calcium response in I2 no more defective than *unc-36* mutants. n = 20.
(R) *unc-36; cca-1* double mutants showed a calcium response in I2 no more defective than *unc-36* mutants. n = 20.
(S) *egl-19; cca-1* double mutants showed a normal calcium response in I2. n = 21.
(T) *unc-36; egl-19; cca-1* triple mutants showed a modest reduction in the calcium response in I2 compared with *unc-36* mutants. n = 27.

(A-G, O-T) Calcium response in the posterior neurite of I2.

Shading around traces indicate s.e.m.

**Figure S3:**

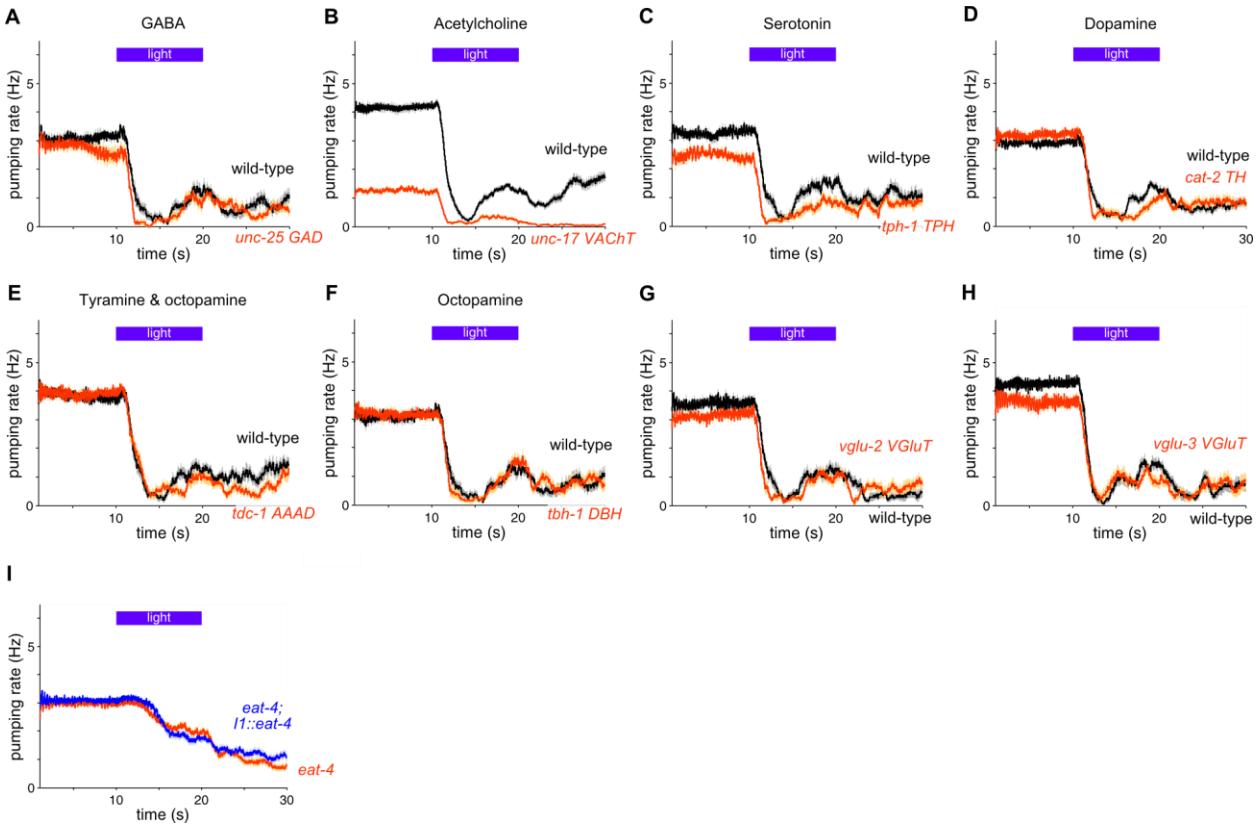


**Figure S3, related to Figure 3. Neurotransmitter mutants with a normal acute response to light, and the failure of I1-specific expression of eat-4 to rescue eat-4 mutants.**

(A) *unc-25(e156) GAD* mutants defective in GABA synthesis showed a normal pumping response to light. 20 °C, n = 20 worms.
(B) *unc-17(e245) VAChT* mutants defective in vesicular acetylcholine import showed a normal acute response to light. 20 and 22.5 °C, n = 80.
(C) *tph-1(n4622) TPH* mutants defective in serotonin synthesis showed a normal acute response to light. 20 °C, n = 20.
(D) *cat-2(e1112) TH* mutants defective in dopamine synthesis showed a normal pumping response to light. 20 °C, n = 40.
(E) *tdc-1(n3420) AAAD* mutants defective in tyramine and octopamine synthesis showed a normal pumping response to light. 20 °C, n = 20.
(F) *tbh-1(n3722) DBH* mutants defective in octopamine synthesis showed a normal pumping response to light. 20 °C, n = 20.
(G) *vglu-2(ok2356) VGluT* mutants defective in glutamate transport showed a normal pumping response to light. n = 20.
(H) *vglu-3(tm3390) VGluT* mutants defective in glutamate transport showed a normal pumping response to light. n = 20.

(I) I1-specific expression of *eat-4* (*gcy-10*$_{prom}$*::eat-4 cDNA::gfp*) failed to rescue the pumping response defect of *eat-4* mutants. n = 60.

Shading around traces indicate s.e.m.

**Figure S4:**

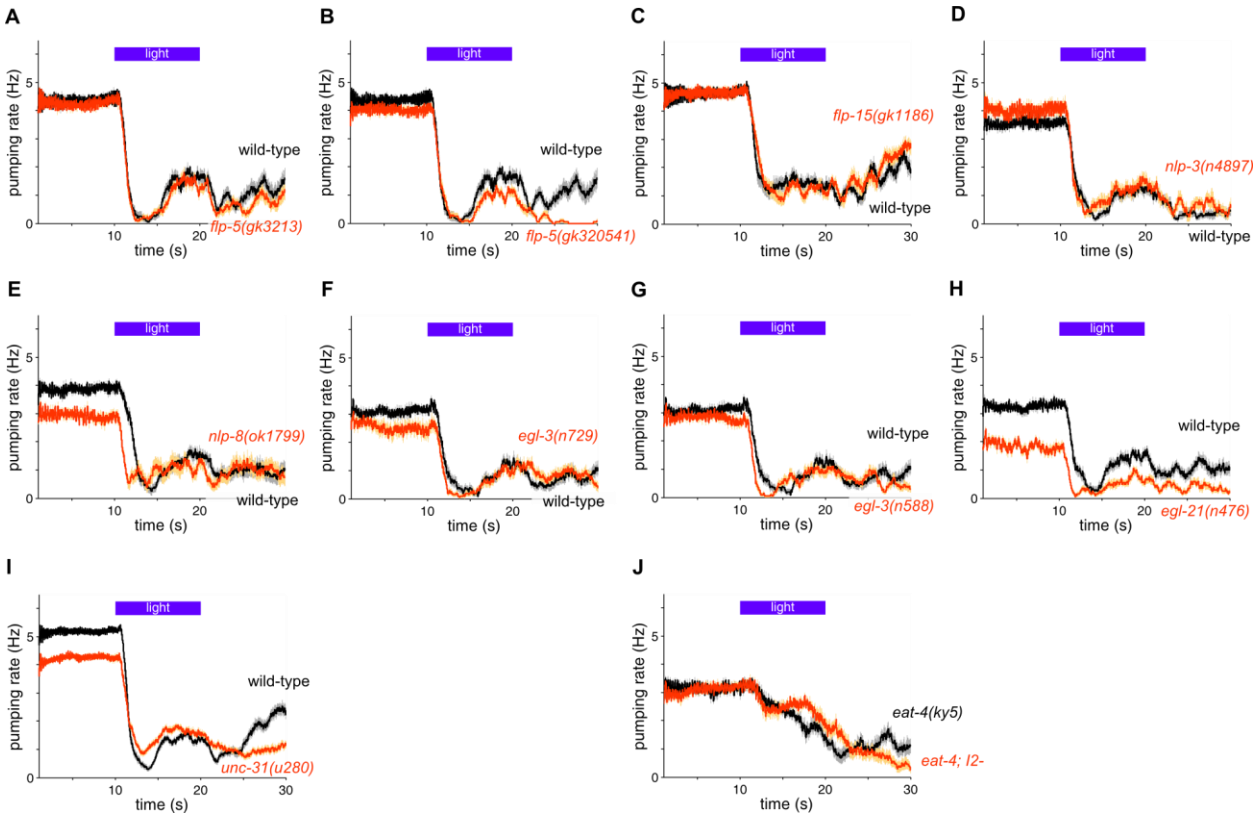


**Figure S4, related to Figure 3: Mutants of neuropeptide genes expressed in I2 have a normal acute response to light, although unc-31 has a defect in the amplitude of the acute response.**

(A) *flp-5(gk3213)* mutants showed a normal pumping response to light. n = 20 worms.
(B) *flp-5(gk320541)* mutants showed a normal acute pumping response to light. n = 20.
(C) *flp-15(gk1186)* mutants showed a normal pumping response to light. n = 20.
(D) *nlp-3(n4897)* mutants showed a normal pumping response to light. n = 20.
(E) *nlp-8(ok1799)* mutants showed a normal pumping response to light. n = 20.
(F) *egl-3(n729)* mutants showed a normal pumping response to light. 20 °C, n = 20.
(G) *egl-3(n588)* mutants showed a normal pumping response to light. 20 °C, n = 20.
(H) *egl-21(n476)* mutants showed a normal acute pumping response to light. 20 °C, n = 20.
(I) *unc-31(u280)* mutants showed a normal acute latency but a defective acute amplitude in response to light ($p < 0.001$, t-test). n = 60.

(J) The acute pumping response defect of *eat-4(ky5)* mutants was not further enhanced by genetic ablation of I2. n = 20.

Shading around traces indicate s.e.m.

**Figure S5:**

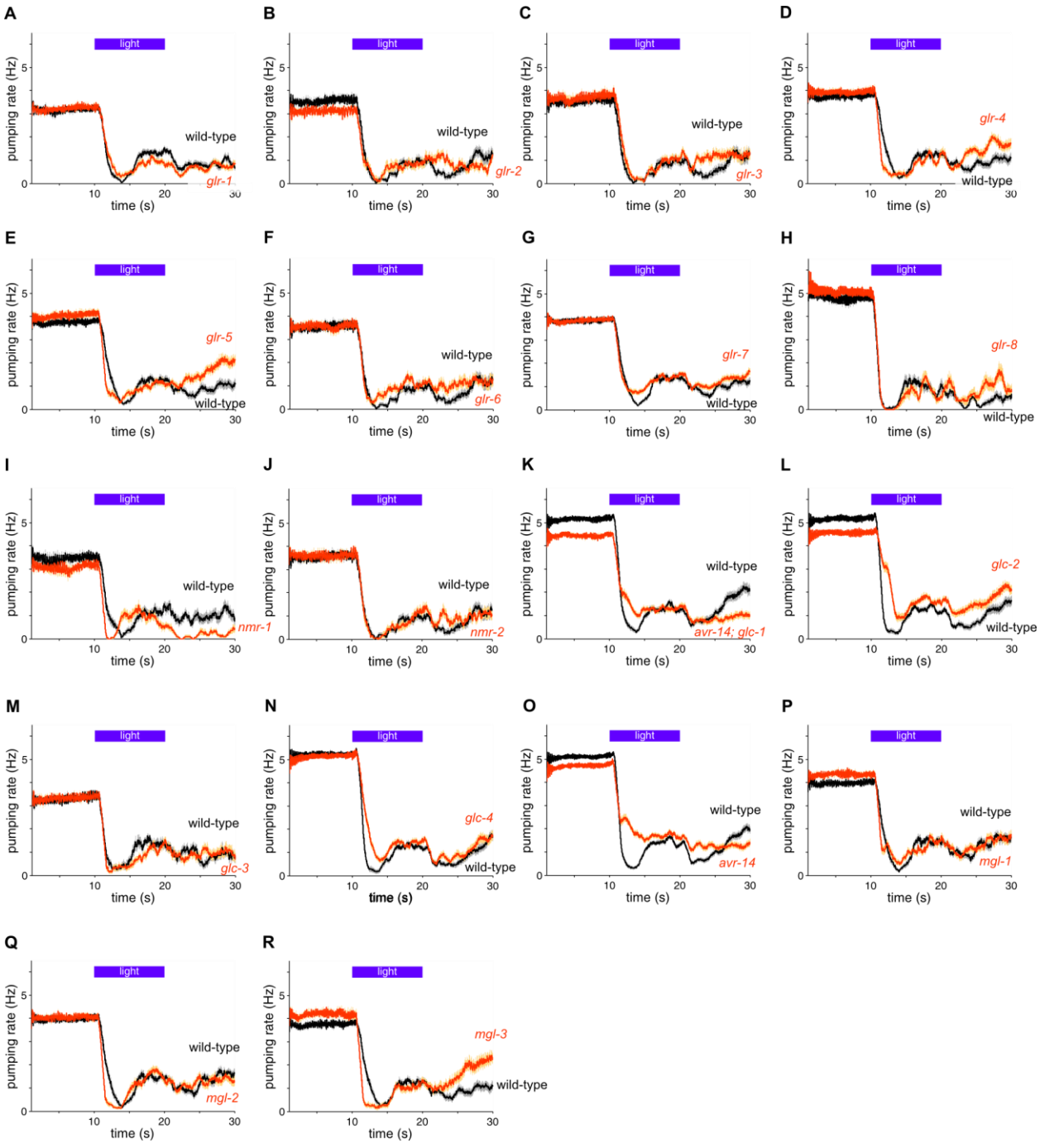


**Figure S5, related to Figure 3. The pumping responses to light of glutamate receptor mutants.**

(A) *glr-1(n2461)* mutants were not defective in their pumping response to light. 20 °C, n = 40 worms.

(B) *glr-2(ak10)* mutants were not defective in their pumping response to light. 20 °C, n = 20.
(C) *glr-3(ak57)* mutants were not defective in their pumping response to light. 20 °C, n = 20.
(D) *glr-4(tm3219)* mutants were not defective in their pumping response to light. n = 40.
(E) *glr-5(tm3506)* mutants were not defective in their pumping response to light. n = 40.
(F) *glr-6(ak56)* mutants were not defective in their pumping response to light. 20 °C, n = 20.
(G) *glr-7(tm2827)* mutants had a normal acute response latency and small but statistically significant reduction in acute response amplitude ($p < 0.05$, t-test). n = 60.
(H) *glr-8(gk283043)* mutants were not defective in their pumping response to light. n = 20.
(I) *nmr-1(ak4)* mutants were not defective in the acute response to light. 20 °C, n = 20.
(J) *nmr-2(ak10)* mutants were not defective in their pumping response to light. 20 °C, n = 20.
(K) *avr-14(ad1302); glc-1(pk54)* mutants had a defective amplitude in the acute response to light. Since *avr-14* single mutants also had an acute response defect of similar magnitude (see O), we attributed the defect in this strain to the *avr-14* mutation. n = 60.
(L) *glc-2(gk179)* mutants had a latency defect in the acute response to light. n = 60.
(M) *glc-3(ok321)* mutants had a normal pumping response to light. 20 °C, n = 20.
(N) *glc-4(ok212)* mutants had a latency defect in the acute response to light. n = 60.
(O) *avr-14(ad1302)* mutants had an amplitude defect in the acute response to light. n = 100.
(P) *mgl-1(tm1811)* mutants were not defective in the pumping response to light. n = 40.
(Q) *mgl-2(tm355)* mutants were not defective in the pumping response to light. n = 40.
(R) *mgl-3(tm1766)* mutants were not defective in the pumping response to light. n = 31.

Shading around traces indicate s.e.m.

# Figure S6 - I2L synapses:

**A** Synapses from I2L (worm #1). All synapses are in the anterior neurite unless specified otherwise. Pharyngeal muscles are underlined.

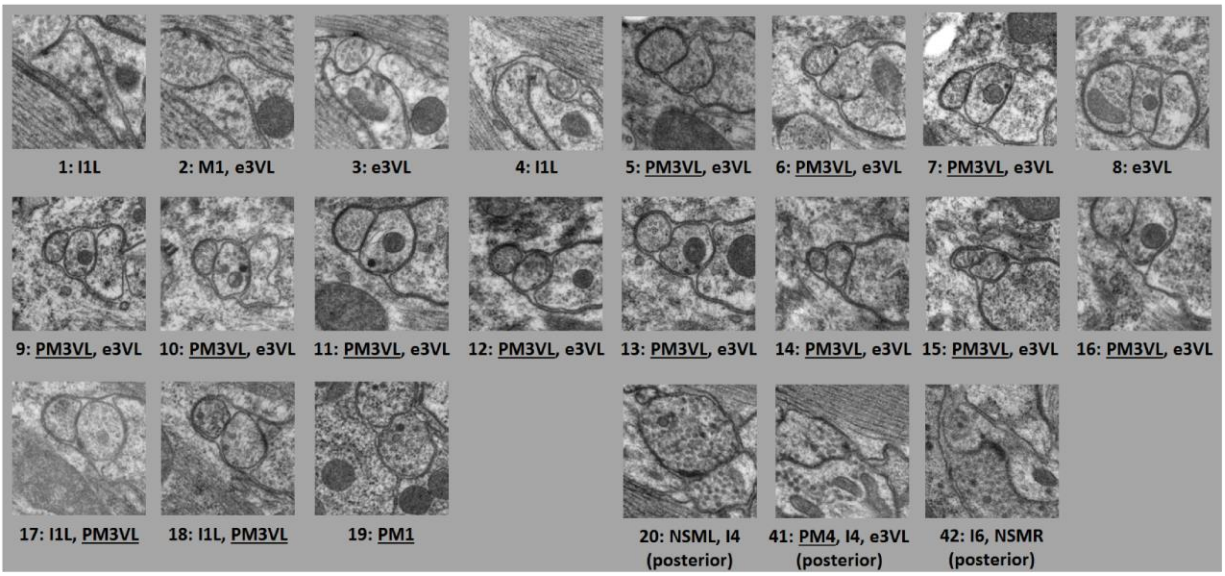


**B** Synapses from I2L (worm #4). All synapses are in the posterior neurite.

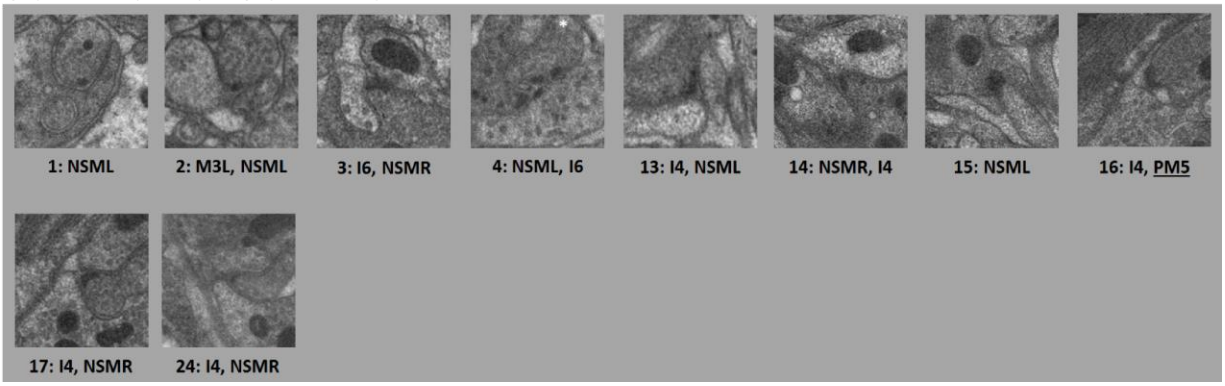

# Figure S6 (cont'd) - I2R synapses:

**C** Synapses from I2R (worm #1). All synapses are in the anterior neurite unless specified otherwise. Pharyngeal muscles are underlined.

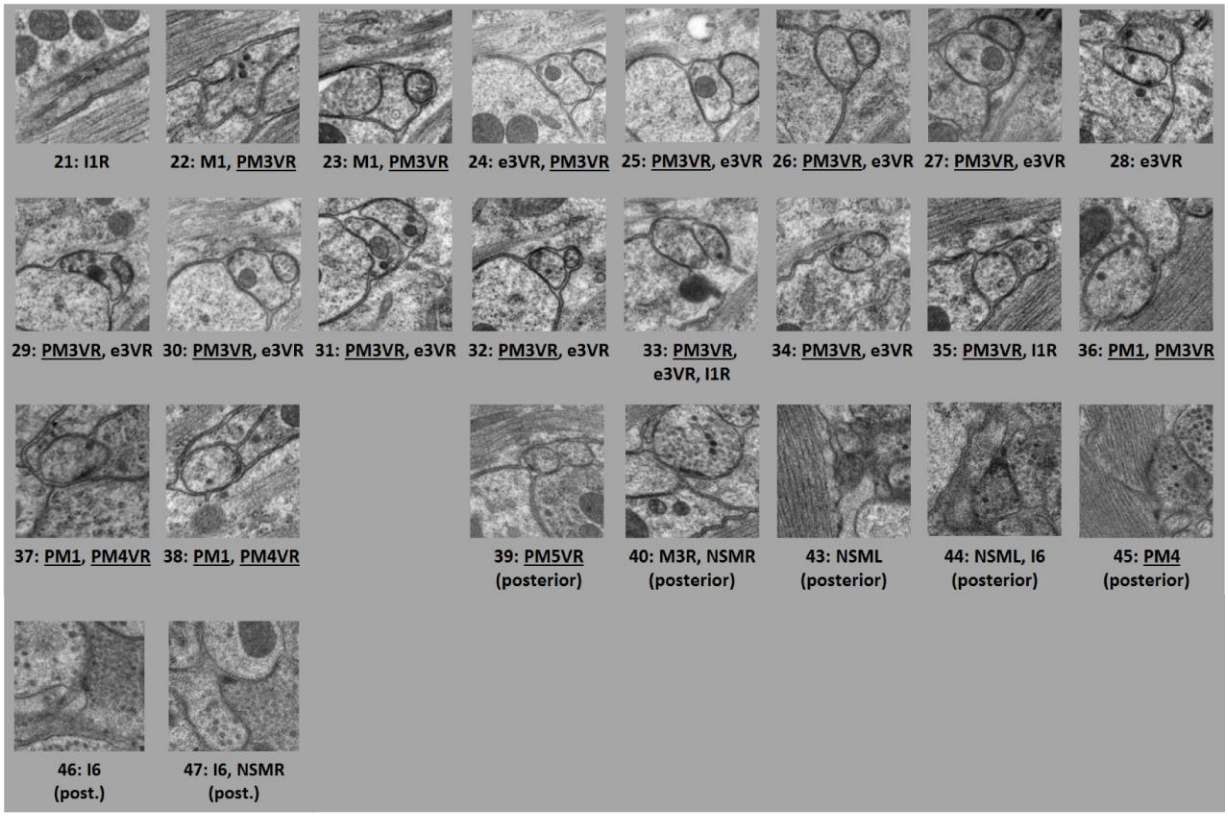


**D** Synapses from I2R (worm #4). All synapses are in the posterior neurite.

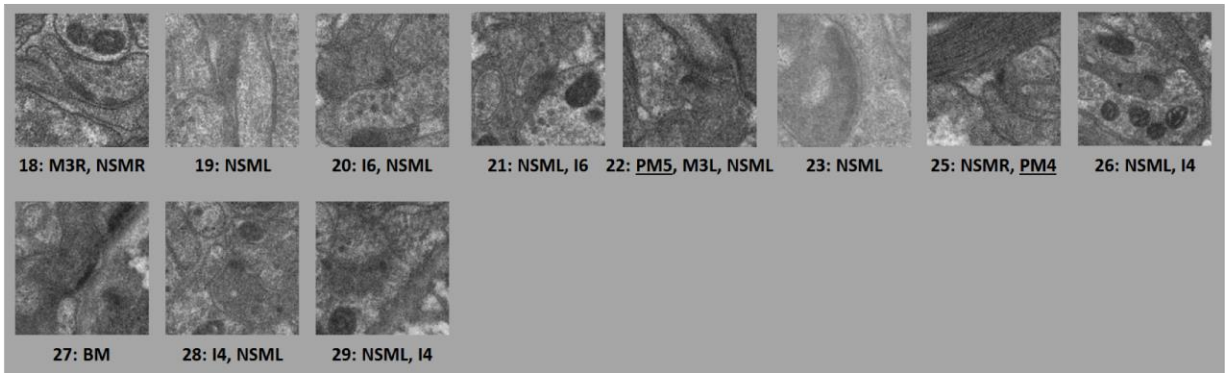

## Figure S6 (cont'd) - Quantification:

**E**

I2L chemical synapses

| | Recipient | # syn. (Albertson) | # syn. (this work) | # sections | DP vol. ($nm^3$) | vesicle area ($nm^2$) |
|---|---|---|---|---|---|---|
| anterior neurite | PM3VL | 0 | 13* | 133 | 893,560 | 318,307 |
| | e3VL | 0 | 14* | 138 | 700,800 | 332,999 |
| | I1L | 0 | 4 | 23 | 361,000 | 84,068 |
| | PM1 | 0 | 1* | 9 | 116,200 | 23,192 |
| | M1 | 1 | 1* | 15 | 0 | 42,168 |
| posterior neurite | NSMR | 3 (L+R) | 4* | 39 | 8,838,700 | nd |
| | I4 | 2 | 5* | 30 | 6,881,600 | nd |
| | NSML | 3 (L+R) | 5* | 22 | 4,306,800 | nd |
| | I6 | 1 | 2* | 17 | 3,918,000 | nd |
| | M3L | 0 | 1* | 5 | 798,300 | nd |
| | PM5 | 0 | 1* | 1 | 408.600 | nd |
| | M1 | 2 | 0 | 0 | 0 | nd |
| | MCL | 1 | 0 | 0 | 0 | nd |

* indicates polyadic synapses were included in the synapse count

I2R chemical synapses

| | Recipient | # syn. (Albertson) | # syn. (this work) | # sections | DP vol. ($nm^3$) | vesicle area ($nm^2$) |
|---|---|---|---|---|---|---|
| anterior neurite | PM1 | 0 | 3* | 13 | 973,400 | 40,288 |
| | PM3VR | 0 | 14* | 108 | 743,900 | 263,264 |
| | PM4VR | 0 | 2* | 7 | 623,300 | 11,156 |
| | e3VR | 0 | 11* | 80 | 405,900 | 180,552 |
| | I1R | 0 | 3* | 19 | 106,300 | 36,492 |
| | M1 | 1 | 2* | 24 | 0 | 59,184 |
| posterior neurite | NSML | 3 (L+R) | 8* | 43 | 12,315,104 | nd |
| | I6 | 1 | 2* | 18 | 4,849,204 | nd |
| | NSMR | 3 (L+R) | 2* | 12 | 3,614,000 | nd |
| | I4 | 2 | 3* | 14 | 2,569,900 | nd |
| | M3R | 0 | 1* | 6 | 2,380,100 | nd |
| | PM4 | 0 | 1* | 6 | 1,233,900 | nd |
| | M3L | 0 | 1* | 5 | 813,500 | nd |
| | PM5 | 0 | 1* | 5 | 813,500 | nd |
| | BM | 0 | 1 | 2 | 503,700 | nd |
| | MCL | 1 | 0 | 0 | 0 | nd |

**Figure S6, related to Figure 4. All I2 synapses observed by electron microscopy.**

(A-D) Electron micrographs of all I2 synapses from two worms. Synapses can span many sections; only a single section is shown for each synapse. The synapse from I2 is in the center of each square micrograph, with the vesicles or presynaptic dense projection near the image center located inside the I2 neuron. In the caption below each square image, the number indicates the synapse ID and the cell names indicate the post-synaptic partners. Within each neuron within each worm, synapses are numbered from anterior to posterior. Underlined cell names indicate pharyngeal muscle.
(A) Electron micrographs of all I2L synapses identified in worm #1. All of the synapses were found in the anterior process of I2L, except when specified otherwise below each image.
(B) Electron micrographs of all I2L synapses identified in worm #4. All of the synapses were found in the posterior process of I2L.
(C) Electron micrographs of all I2R synapses identified in worm #1. All of the synapses were found in the anterior process of I2R, except when specified otherwise below each image.
(D) Electron micrographs of all I2R synapses identified in worm #4. All of the synapses were found in the posterior process of I2R.
(E) Table showing measurements for all I2 synapses identified in electron micrographs. The anterior neurites, soma and part of the posterior neurites were reconstructed from one adult hermaphrodite (worm #1), and the soma and posterior neurites were reconstructed from a second adult hermaphrodite (worm #4). The anterior synapses were confirmed by sparsely sampling a third worm (worm #5, data not shown). In the table, quantification of the anterior synapses was from worm #1, and quantification of the posterior synapses was from worm #4. The second column shows the number of synapses previously reported by Albertson and Thomson (1976), while the third column shows the number of synapses identified in this work. The fourth column shows the number of EM sections over which all of the synapses onto the recipient were distributed. Dense projection (DP) volumes and vesicle areas were calculated using the Measure feature of TrakEM2 [S1]. The listed DP volumes and vesicle areas are the sum of these values across all synapses with the specific partners indicated by the row in the table. * indicates that the synapse count included polyadic synapses in which the I2 synapse opposed more than one

cell. nd = not determined, BM = basement membrane. For post-synaptic partners NSML and NSMR, Albertson and Thomson (1976) did not distinguish whether the left or right NSM received the synapse from I2.

**Figure S7:**

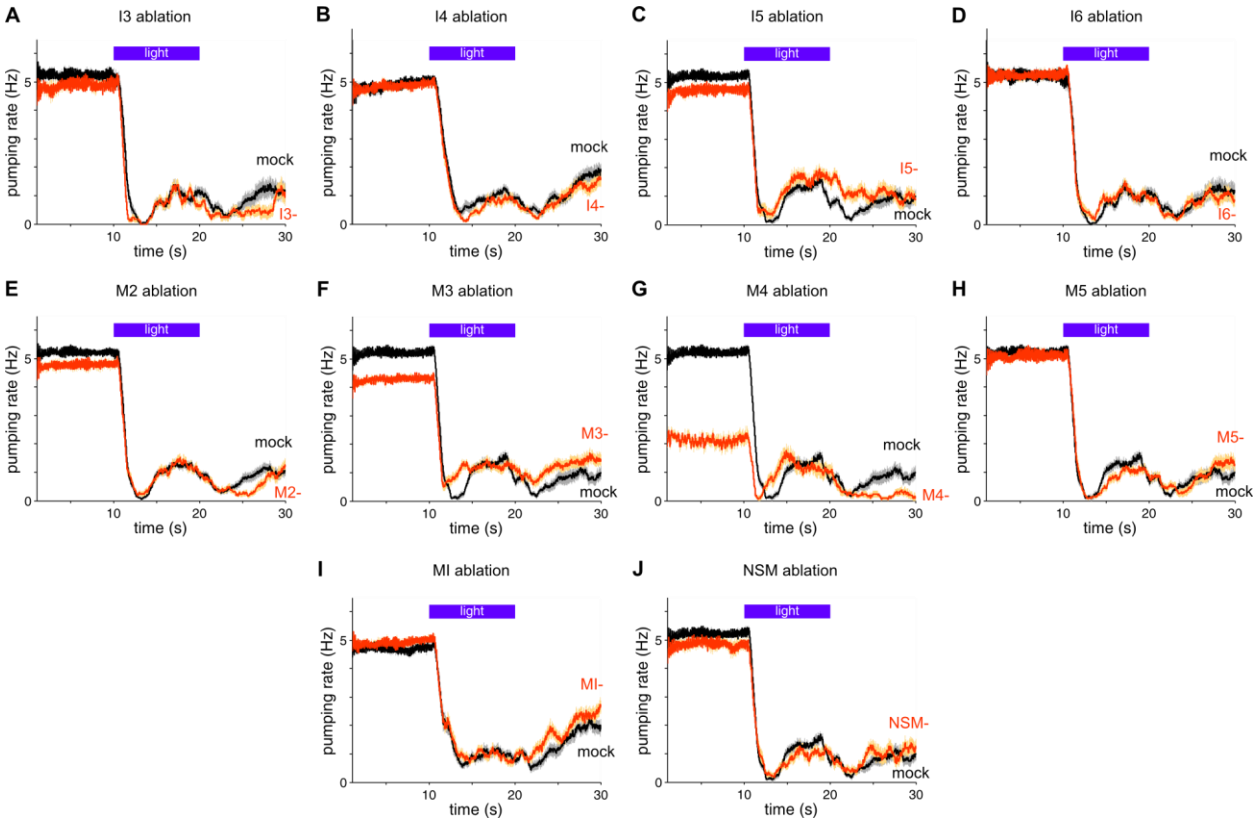


**Figure S7, related to Figure 5. The effect of individual laser ablation of the remaining pharyngeal neurons on the pumping response to light.**

(A) Ablation of the I3 neuron did not affect the pumping response to light. n = 18 trials, 6 worms.
(B) Ablation of the I4 neuron did not affect the pumping response to light. n = 30 trials, 12 worms. Reproduced from [S2].
(C) Ablation of the I5 neuron did not affect the pumping response to light. n = 26 trials, 9 worms.
(D) Ablation of the I6 neuron did not affect the pumping response to light. n = 27 trials, 10 worms.
(E) Ablation of the M2 neuron pair did not affect the pumping response to light. n = 35 trials, 11 worms.
(F) Ablation of the M3 neuron pair did not affect the acute response latency and caused a small but statistically significant defect in the acute response amplitude ($p < 0.001$, t-test). n = 37 trials, 13 worms.
(G) Ablation of the M4 neuron did not affect the acute or burst responses to light. n = 21 trials, 7 worms.
(H) Ablation of the M5 neuron did not affect the pumping response to light. n = 35 trials, 11 worms.

(I) Ablation of the MI neuron did not affect the pumping response to light. n = 34 trials, 13 worms.
(J) Ablation of the NSM neuron pair did not affect the pumping response to light. n = 23 trials, 8 worms.

Shading around traces indicate s.e.m.

## SUPPLEMENTAL EXPERIMENTAL PROCEDURES

### Strains

The following *C. elegans* strains were used (in order of mention):

N2 (wild-type)
MT21650 *nIs575[flp-15$_{prom}$::gcamp3; lin-15(+)]; lin-15(n765)*
MT21635 *nIs571[flp-15$_{prom}$::gcamp3; lin-15(+)]; lin-15(n765)*
MT21431 *nIs572[flp-15$_{prom}$::gcamp3; lin-15(+)]; lin-15(n765)*
MT21644 *nIs575; unc-31(u280); lin-15(n765)*
MT1212 *egl-19(n582)*
MT21639 *nIs575; egl-19(n582); lin-15(n765)*
CB55 *unc-2(e55)*
MT21652 *nIs575; unc-2(e55) lin-15(n765)*
JD21 *cca-1(ad1650)*
MT21787 *nIs575; cca-1(ad1650) lin-15(n765)*
CB251 *unc-36(e251)*
MT21637 *nIs571; unc-36(e251); lin-15(n765)*
VC550 *tag-180(ok779)*
MT21653 *tag-180(ok779); nIs575; lin-15(n765)*
VC12 *unc-77(gk9)*
MT21900 *nIs575; unc-77(gk9); lin-15(n765)*
VC9 *nca-2(gk5)*
MT21901 *nIs571; nca-2(gk5); lin-15(n765)*
CB540 *unc-68(e540)*
MT21651 *nIs575; unc-68(e540); lin-15(n765)*
JT73 *itr-1(sa73)*
MT21766 *nIs575; itr-1(sa73); lin-15(n765)*
MT21780 *nIs571; unc-36(e251); unc-2(e55) lin-15(n765)*
MT23567 *nIs575; egl-19(n582); unc-2(e55) lin-15(n765)*
MT23574 *nIs575; unc-2(e55) cca-1(ad1650) lin-15(n765)*
MT23569 *nIs571; unc-36(e251); egl-19(n582); lin-15(n765)*
MT23575 *nIs571; unc-36(e251); cca-1(ad1650) lin-15(n765)*
MT23578 *nIs575; egl-19(n582); cca-1(ad1650) lin-15(n765)*
MT23582 *nIs572; unc-36(e251); egl-19(n582); cca-1(ad1650) lin-15(n765)*
CB156 *unc-25(e156)*
CB933 *unc-17(e245)*
MT14984 *tph-1(n4622)*
CB1112 *cat-2(e1112)*
MT10548 *tdc-1(n3420)*
MT11374 *tbh-1(n3722)*
RB1821 *vglu-2(ok2356)*
FX03990 *vglu-3(tm3990)*
MT6308 *eat-4(ky5)*
MT6302 *eat-4(n2458)*

MT6318 *eat-4(n2474)*
DA819 *eat-4(ad819)*
DA572 *eat-4(ad572)*
MT20669 *eat-4(ok2233)*
IK883 *eat-4(ky5); njEx378[eat-4$_{prom}$::eat-4::gfp; ges-1$_{prom}$::gfp]*
MT21211 *eat-4(ky5); lin-15(n765); nIs529[flp-15$_{prom}$::eat-4 cDNA::gfp; lin-15(+) #1]*
MT21212 *eat-4(ky5); lin-15(n765); nIs530[flp-15$_{prom}$::eat-4 cDNA::gfp; lin-15(+) #2]*
MT21213 *eat-4(ky5); lin-15(n765); nIs531[flp-15$_{prom}$::eat-4 cDNA::gfp; lin-15(+) #3]*
MT21206 *eat-4(ky5); lin-15(n765); nIs524[gcy-10$_{prom}$::eat-4 cDNA::gfp; lin-15(+)]*
MT20722 *lite-1(ce314)*
MT20728 *eat-4(ky5); lite-1(ce314)*
MT21563 *eat-4(ky5); lite-1(ce314) lin-15(n765); nIs530*
VC3280 *F15A4.3(gk3259); flp-5(gk3123)*
VC20382 *flp-5(gk320541)*
VC2504 *flp-15(gk1186)*
MT15951 *nlp-3(n4897)*
VC1309 *nlp-8(ok1799)*
MT1541 *egl-3(n729)*
MT1218 *egl-3(n588)*
MT1071 *egl-21(n476)*
TU280 *unc-31(u280)*
MT22819 *eat-4(ky5); nIs569[flp-15$_{prom}$::csp-1b cDNA; ges-1$_{prom}$::gfp]*
MT6305 *glr-1(n2461)*
VM1390 *glr-2(ak10)*
VM1846 *glr-3(ak57)*
FX3239 *glr-4(tm3239)*
FX3506 *glr-5(tm3506)*
VM685 *glr-6(ak56)*
FX2877 *glr-7(tm2877)*
VC20465 *glr-8(gk283043)*
VM487 *nmr-1(ak4)*
VM6310 *nmr-2(ak7)*
DA1384 *avr-14(ad1302); glc-1(pk54)*
VC350 *glc-2(gk179)*
XA7400 *glc-3(ok321)*
JD31 *glc-4(ok212)*
DA1371 *avr-14(ad1302)*
FX1811 *mgl-1(tm1811)*
FX355 *mgl-2(tm355)*
FX1766 *mgl-3(tm1766)*
JD105 *avr-15(ad1051)*
MT22171 *avr-15(ad1051); lin-15(n765); nEx2149[myo-2$_{prom}$::avr-15A cDNA; lin-15(+)]*
OH4887 *otIs182[inx-18$_{prom}$::gfp]*
PS3504 *syIs54[ceh-2$_{prom}$::gfp, unc-119(+)]; unc-119(ed4)*
MT17641 *nIs264[gcy-10$_{prom}$::4xNLS::gfp, lin-15(+)]; lin-15(n765)*
MT17912 *nIs282[gcy-10$_{prom}$::4xNLS::gfp, lin-15(+)]; lin-15(n765)*

NL2334 *pkIs1273[gpa-16$_{prom}$::gfp]*
MT21198 *nEx1997[gpa-16$_{prom}$::gfp; unc-54$_{prom}$::rfp]*
MT23561 *nIs552[gcy-10$_{prom}$::chr2::yfp; lin-15(+)]; lite-1(ce314) gur-3(ok2245) lin-15(n765)*
MT21419 *nIs560[gcy-10$_{prom}$::enphr3::yfp; lin-15(+)]; lin-15(n765)*
MT23594 *nIs551[gcy-10$_{prom}$::chr2::yfp; lin-15(+)]; nIs711[flp-21$_{prom}$::gcamp3; lin-15(+)]; lite-1(ce314) gur-3(ok2245) lin-15(n765)*
MT23595 *nIs552; nIs711; lite-1(ce314) gur-3(ok2245) lin-15(n765)*

**Molecular biology**

We used the following primers to amplify DNA for generating transgenes by restriction enzyme cloning or PCR fusion. For cDNA, wild-type mixed-stage poly-A RNA was used as template.

| | |
|---|---|
| *flp-15$_{prom}$*: | TGAACTTTCCTCATTTCCCCTTCGTTC, GACGAGGTGTATGTGGGAGACC |
| *eat-4 cDNA*: | ATGTCGTCATGGAACGAGGCTTG, CCACTGCTGATAATGCGGATTTTCC |
| *myo-2$_{prom}$*: | GTGTTGTGTATAGTGTACGAGAAAATGGAG, TTCTGTGTCTGACGATCGAGGGT |
| *avr-15A cDNA*: | ATGATAGGTCGATTGCGGAGAGG, CGTACTGATGGCCACACCGTATTG |
| *gcy-10$_{prom}$* [S3]: | TGGGTACAACAATTTCTCATTCAAATT, TTTGAGCAGAAGGCCAATTATCGAAAAG |
| *flp-21$_{prom}$* [S4]: | AACTAGGTCCAGTGACCGAAAGTG, CGTCTGAAAATGACTTTTTGGATTTTGGAG |

**Light-induced pumping response**

This assay was conducted as previously described [S2]. Briefly, 1 day-old adult hermaphrodites were placed on a seeded NGM agar plate. Pumping was scored by eye using a stereo dissecting microscope set to 120x magnification and illuminated with a halogen transmitted light source (Zeiss Lumar and KL 2500 LCD, 3100 K). Custom Matlab software (available at www.wormweb.org) recorded the timing of pumps as indicated by manual key presses and controlled a shutter (via a Zeiss EMS-1 controller) that presented and removed mercury arc epi-illumination (HBO 100). We used a modified CFP filterset (Zeiss Lumar filter set 47 HE CFP

486047) to illuminate 436 ± 13 nm violet light at an intensity of 13 mW/mm$^2$. All experiments were done at 22.5 °C, unless specified otherwise. Data generated by real-time scoring was previously confirmed for wild-type and I2-ablated animals by video analysis [S2]. When assaying wild-type and mutant strains, each worm was assayed once. When assaying mock-ablated, ablated and ATR± worms, each worm was assayed 1-4 times.

**Pharyngeal transport assay**

To visualize the direction of flow in the pharynx for each pump, worms were fed either a 50% dilution of 1 µm polystyrene beads in M9 (Polysciences) or mineral oil. 1 day-old adults were placed with bacteria on an NGM agar pad on a coverslip and observed with a 20x objective on an inverted microscope (Zeiss Axiovert S100). Videos were recorded at 1000 fps using a high-speed camera (Photron Fastcam SA3), except that experiments with mineral oil were recorded at 86 fps using an EMCCD camera (Andor iXon+). 436 nm light (10 mW/mm$^2$; Till Photonics Polychrome V, 150 W Xenon bulb) was presented to the worm for 10 s. Videos were viewed and manually annotated, using custom Matlab software, for specific behavioral events: ingestion (beads being retained in the corpus after corpus relaxation), spitting (beads flowing out of the corpus), and pumping (movement of the grinder). In some cases, the worm moved out of the field-of-view of the camera, in which case those frames were annotated as "missing" and excluded from further analysis.

**Behavioral statistics**

Behavioral statistics were calculated as described previously [S2]. Briefly, the acute response latency is the time between the onset of light and the first missed pump. The first missed pump

is determined by identifying the first time interval between pumps that exceeds twice the pre-light pumping rate for that animal. The acute response amplitude is the rate of pumping in the first 3 s following the first missed pump divided by the pre-light pumping rate. The burst response amplitude is the rate of pumping in the last 5 s of light exposure divided by the pre-light pumping rate. Spitting rate was calculated as follows. First, for individual worms the spitting rate was calculated as the number of spits divided by the duration of light exposure, with "missing" frames excluded. Second, the spitting rate for a set of worms of a given condition was calculated as the weighted average of the individual worms' spitting rates, where the weight was determined as the fraction of the time that the worm was not missing from the field-of-view.

**Laser ablations**

We used a pulsed nitrogen laser to conduct laser microsurgery of individual pharyngeal neurons (Laser Science, Inc. VSL-337 attached to a Zeiss Axioplan microscope), as previously described [S5,S6]. Briefly, worms were immobilized by 10 mM sodium azide and mounted for viewing through a 100x oil objective. In general, ablations were performed on larvae of stage 1 or 2 (L1 or L2), with cells identified by nucleus location visualized with either Nomarski differential interference contrast optics or a cell-specific GFP reporter. Ablation of the M4 neuron was performed on larvae of stage 3 (L3), as the worms were more likely to grow to adulthood when ablated at this later stage. Ablations were confirmed the following day by appearance under Nomarski optics or by the loss of cell-specific fluorescence. On day 3 or 4, adults were assayed for their response to light.

**Calcium imaging**

We assayed the calcium response to light of the I2 neuron as previously described [S2]. Briefly, worms were immobilized using high friction [S7]. In our standard assay for I2, the worm was simultaneously imaged and stimulated with 26 $mW/mm^2$ 485 nm blue light for 7 s, and videos were recorded at 15 fps. Frames of each video were aligned to minimize motion using the ImageJ plugin StackReg and analyzed for changes in fluorescence using manually drawn regions-of-interest (ROIs) and a custom Matlab program (available at www.wormweb.org). The latency of the calcium response of I2 was determined as the time from light onset to a fluorescence level greater than or equal to 20% above the baseline fluorescence level (i.e. 20% $\Delta F/F_0$). The amplitude of the calcium response of I2 was determined as the maximum GCaMP3 fluorescence observed during the duration of light stimulation/imaging. Outliers were excluded, such as if the I2 neuron was dark at baseline or did not respond to light exposure. For spatial analysis, we used a laser-scanning confocal microscope (Zeiss LSM 510) to selectively stimulate regions of the head with the 488 nm emission from a 25 mW argon laser. Videos were recorded at low resolution (128x128) so that a high frame rate could be sustained (5 fps). A 40x water objective was used. Worms were imaged for 2 s at 2% laser power, then an ROI was stimulated for 0.16 s (axon), 0.12 s (soma), or 0.62 s (dendrite) at 100% laser power, followed by imaging for 8 s. The duration of exposure for each ROI varied because the area of illumination varied, with each pixel in each ROI exposed for the same duration. For calcium imaging of MC, M4 and M2, the imaging conditions were the same as for I2 imaging except videos were recorded for a duration of 15 s. For the MC neurite, the posterior ventral neurite was analyzed only if it was separate from the M4 and M2 ventral neurites. The 485 nm light used for imaging also caused activation of ChR2. Since MC, M4 and M2 showed repeated calcium oscillations, a custom Matlab script analyzed the fluorescence changes and identified each likely calcium spike, which

was manually confirmed. The calcium peak amplitude was calculated as the difference between the fluorescence peak level and the lowest fluorescence level observed since the last peak. Changes in fluorescence due to changes in calcium could be distinguished from changes due to the motion caused by pumping by the fluorescence amplitude: pumping caused small transients superimposed on the larger transients caused by calcium changes. Only the first large fluorescence transient was included for analysis. For all calcium imaging assays, a single neuron of each class was assayed per animal, and each animal was assayed only once.

**Optogenetic depolarization and hyperpolarization**

Cultivation plates were seeded with 300 µl of OP50 *E. coli* mixed with 0.5 µl of 100 mM all-*trans* retinal (ATR+) or ethanol alone (ATR-) and incubated at room temperature for one day prior to placement of worms. Transgenic worms carrying channelrhodopsin (ChR2) [S8,S9] fused to yellow fluorescent protein (YFP) or halorhodopsin (eNpHR3) [S10] fused to YFP were cultivated on these plates in the dark from egg to adulthood. For ablation experiments, worms were cultivated with ATR± after ablation as L2 larvae. For behavioral assays, ChR2-expressing one day-old adults were illuminated after picking to plates lacking food, which retained a small amount of bacteria. eNpHR3-expressing worms were illuminated on the cultivation plate. We used a GFP filterset (Zeiss Lumar filter set 38 HE GFP 486038) to activate ChR2 with 470 ± 20 nm blue light at 1.5 mW/mm$^2$, and we used an RFP filterset (Zeiss Lumar filter set 43 HE RFP 486043) to activate eNpHR3 with 550 ± 13 nm green light at 10 mW/mm$^2$. To calculate the pumping rate during light exposure, the total pumps during light exposure were divided by the time interval of light exposure (10 s). For optogenetics with calcium imaging, see the "Calcium imaging" section above.

**Expression analysis**

To observe gene expression of *njEx378[eat-4$_{prom}$::eat-4::gfp]* in I2, images were recorded using a light microscope (Zeiss Axioskop 2) and a CCD camera (Hamamatsu ORCA-ER).

**Electron microscopy**

Adult N2 worms were loaded into a Type A carrier coated with 1-hexadecene and filled with a slurry of OP50 *E. coli*, then covered with a Type B carrier [S11]. The sandwich was placed into the specimen holder and frozen using a high pressure freezer (Abra HPM010). Samples were substituted with 1% $OsO_4$, 0.2% uranyl acetate in 95% acetone::5% methanol at -90 °C for 110 h, warmed to -20 °C over 14 h, held at -20 °C for 16 h and warmed to 0 °C over 3.3 h (RMC FS-2500) [S12]. Samples were washed three times with acetone at 0 °C and three times at room temperature before stepwise infiltrated with Eponate 12 resin (Ted Pella) and polymerized at 65 °C. Individually embedded worms were thin-sectioned and imaged with a transmission electron microscope (JEOL JEM-1200 ExII) and CCD camera (AMT XR1241) at multiple magnifications (5,000x, 10,000x, 40,000x). Section thickness varied between 40-50 nm, with the 5,000x magnification images spanning a 30 x 30 µm area. Images were cropped to remove captions, automatically aligned using TrakEM2 [S1] in Fiji, and then the alignment was manually corrected. Cells in the anterior pharynx were manually traced. Synapses from the I2 neurons were annotated if more than two vesicles were present near the membrane or a clearly visible dense projection was present in the absence of vesicles. Dense projections were manually annotated, and their volumes were quantified using the Measure feature of TrakEM2. Synaptic vesicles were manually annotated, and their areas were quantified using the Measure feature of

TrakEM2. Synapse size was calculated as the sum of the dense projection volume and volumes of synaptic vesicles, using the average vesicle diameter we observed, 30 nm; this method was applied uniformly whether the synaptic output was to a single partner or multiple partners (polyadic).

**Supplemental References**


[S1] Cardona, A., Saalfeld, S., Schindelin, J., Arganda-Carreras, I., Preibisch, S., Longair, M., Tomancak, P., Hartenstein, V. & Douglas, R. J. (2012). TrakEM2 software for neural circuit reconstruction. PLoS One *7*, e38011.

[S2] Bhatla, N. & Horvitz, H. R. (2015). Light and hydrogen peroxide inhibit *C. elegans* feeding through gustatory receptor orthologs and pharyngeal neurons. Neuron *85*, 804-818.

[S3] Yu, S., Avery, L., Baude, E. & Garbers, D. L. (1997). Guanylyl cyclase expression in specific sensory neurons: A new family of chemosensory receptors. Proceedings of the National Academy of Sciences *94*, 3384-3387.

[S4] Rogers, C., Reale, V., Kim, K., Chatwin, H., Li, C., Evans, P. & de Bono, M. (2003). Inhibiton of *Caenorhabditis elegans* social feeding by FMRFamide-related peptide activation of NPR-1. Nature Neuroscience *6*, 1178-1185.

[S5] Bargmann, C. I. & Avery, L. (1995). Laser killing of cells in *Caenorhabditis elegans*. In Methods in Cell Biology, Epstein, H. F. & Shakes, D. C., ed. (San Diego: Academic Press), pp. 225-250.

[S6] Fang-Yen, C., Gabel, C. V., Samuel, A. D. T., Bargmann, C. I. & Avery, L. (2012). Laser Microsurgery in *Caenorhabditis elegans*. In *Caenorhabditis elegans*: Cell Biology and Physiology, Rothman, J. H. & Singson, A., ed. (Boston: Academic Press), pp. 177-206.

[S7] Kim, E., Sun, L., Gabel, C. V. & Fang-Yen, C. (2013). Long-term imaging of *Caenorhabditis elegans* using nanoparticle-mediated immobilization. PLoS One *8*, e53419.

[S8] Boyden, E. S., Zhang, F., Bamberg, E., Nagel, G. & Deisseroth, K. (2005). Millisecond-timescale, genetically targeted optical control of neural activity. Nature Neuroscience *8*, 1263-1268.

[S9] Nagel, G., Brauner, M., Liewald, J. F., Adeishvili, N., Bamberg, E. & Gottschalk, A. (2005). Light activation of Channelrhodopsin-2 in excitable cells of *Caenorhabditis elegans* triggers rapid behavioral responses. Current Biology *15*, 2279-2284.

[S10] Gradinaru, V., Zhang, F., Ramakrishnan, C., Mattis, J., Prakash, R., Diester, I., Goshen, I., Thompson, K. R. & Deisseroth, K. (2010). Molecular and cellular approaches for

diversifying and extending optogenetics. Cell *141*, 154-165.

[S11] Hall, D. H., Hartweig, E. & Nguyen, K. C. Q. (2012). Modern Electron Microscopy Methods for *C. elegans*. In Methods in Cell Biology, Rothman, J. H. & Singson, A., ed. (San Diego: Academic Press), pp. 93-149.

[S12] Fetter, R. (2013). High pressure freeze of embryos and L1s, Available at http://www.wormatlas.org/EMmethods/Highpressurefreezeembryo.htm.